INSTITUTE OF PHYSICS PUBLISHING and INTERNATIONAL ATOMIC ENERGY AGENCY NUCLEAR FUSION

Nucl. Fusion **45** (2005) 297–317 doi:10.1088/0029-5515/45/5/001

Characterization of small ELM experiments in highly shaped single null and quasi-double-null plasmas in JET

G. Saibene[1], P.J. Lomas[2], R. Sartori[1], A. Loarte[1], J. Stober[3], Y. Andrew[2], S.A. Arshad[2,4], G.D. Conway[3], E. de la Luna[5], K. Günther[2], L.C. Ingesson[6,1], M.A.H. Kempenaars[6], A. Korotkov[2], H.R. Koslowski[7], J.S. Lönnroth[8], D.C. McDonald[2], A. Meigs[2], P. Monier-Garbet[9], V. Parail[2], C.P. Perez[7], F.G. Rimini[9], S. Sharapov[2] and P.R. Thomas[9]

[1] EFDA Close Support Unit, Boltzmannstr. 2, 85748 Garching, Germany
[2] Association Euratom/UKAEA, Culham Science Centre, Abingdon OX14 3EA, UK
[3] Association Euratom/IPP, MPI fur Plasmaphysik, 2 Boltzmannstrasse, Garching, Germany
[4] EFDA Close Support Unit JET, Culham Science Centre, Abingdon OX14 3EA, UK
[5] Asociación Euratom-CIEMAT, Avenida Complutense 22, E-28040 Madrid, Spain
[6] FOM/Euraton instituut v plasmaphysica 'Rijnhuizen', Nieuwegein, Trilateral Euregio Cluster, The Netherlands
[7] Forschungszentrum Jülich GmbH, Institut für Plasmaphysik, EURATOM Association, Trilateral Euregio Cluster, 52425 Jülich, Germany
[8] Association EURATOM-Tekes, Helsinki University of Technology, PO Box 2200, 02015 HUT, Finland
[9] Association Euratom/CEA, Cadarache, F13108 St. Paul-lez-Durance, France

Received 24 November 2004, accepted for publication 16 March 2005
Published 26 April 2005
Online at stacks.iop.org/NF/45/297

Abstract
This paper describes experiments with highly shaped JET H-mode plasmas, which were directed to developing regimes where Type I ELMs are replaced by other edge relaxations, while maintaining the pedestal pressure of Type I ELMy H-modes. It was found that Type II ELMs coexisted with Type I, up to densities of the order of the Greenwald limit, where Type III ELMs appear, and the good confinement was lost. Only at the highest edge collisionality was it observed that Type II ELMs completely replace Type I. At high β_p and q_{95}, 'grassy' ELMs replace Type I completely. The MHD spectra characteristics for grassy ELMs are significantly different from those of Type II ELMs. This paper details the experiments, briefly compares the results to those obtained elsewhere and suggests open lines of investigations for the assessment of the potential of grassy ELM regimes as an ELM mitigation technique.

PACS numbers: 52.55.Fa and 52.55.Tn

1. Introduction

Access conditions and plasma performance of H-modes with acceptable ELM size (extrapolated to ITER conditions (Federici *et al* 2003)) have been one of the main research lines in recent experimental campaigns at JET. This paper describes experiments dedicated to the study of pedestal and ELM behaviour of high density/high confinement ELMy H-modes (Saibene *et al* 2002, Loarte *et al* 2004), focusing on the exploration of access conditions for small ELM regimes without the use of 'external actuators', such as, for example, repetitive pellet injection (Lang *et al* 2003) or edge magnetic perturbation coils (Evans *et al* 2004).

Regimes combining high global confinement, high pedestal pressure p_{ped} and small ELMs have been achieved in ASDEX Upgrade and JT-60U: in both cases, a spontaneous transition from a standard ELMy H-mode edge is observed, in response to changes in some specific plasma parameters. In the case of ASDEX Upgrade, (Stober *et al* 2001) Type II ELMs replace Type I ELMs when the plasma magnetic configuration is changed from lower single null (SN) to quasi-double-null (QDN). For standard ELMy H-modes ($\beta_N \sim 1.8$–2.2), high

pedestal density ($n_{\rm ped} \gtrsim$ 6–7 $\times 10^{19}\,{\rm m}^{-3}$ or 60–70%$n_{\rm GR}$, with $n_{\rm GR} = I_p/\pi a^2$, $10^{20}\,{\rm m}^{-3}\,{\rm MA}$, where I_p is the plasma current and a the plasma minor radius (Greenwald *et al* 1988)), edge safety factor $q_{95} \gtrsim$ 4.0–4.5 and high triangularity are also required for the transition to take place, but they are not sufficient conditions. The identification of Type II ELMs is subtle since no simple criterion (such as ELM frequency versus power, used for Type I and III) has been found. During Type II ELMs, the large, periodic D_α spikes characteristic of Type I ELMs disappear and are substituted by small and irregular oscillations. The pedestal pressure is almost unchanged (in contrast to what happens in a Type I to Type III ELM transition), and, in the case of pure Type II ELMs H-modes (i.e. with complete Type I ELM suppression), both pedestal temperature and density reach steady state. Finally, Type II ELMs are accompanied by edge-localized broadband MHD turbulence, rotating in the electron diamagnetic drift direction, and occur at relatively high pedestal collisionality ($\nu_e^* \sim 1$). Type II ELMy edge (with some residual Type I ELM activity) is also obtained in ASDEX Upgrade in the 'improved' H-mode regime (Sips *et al* 2002). In this case, ν^* can be as low as 0.5 and the minimum q_{95} is reduced to 3.5.

In the case of JT-60U (Kamada *et al* 2002), high triangularity ($\delta \sim$ 0.45–0.7) ELMy H-modes with medium–high q_{95} ($q_{95} \sim$ 3.8–6) enter a regime characterized by high $p_{\rm ped}$ and small ELMs (named 'grassy ELMs' regime) when a β_p threshold of ∼1.6–1.7 is exceeded. As for Type II ELMs, no simple phenomenological identification criteria exist: the signature on the divertor D_α emission, is similar to that of Type II ELMs and the pedestal pressure is also similar to comparable plasmas with a Type I ELMy edge. In contrast to Type II ELMs, grassy ELMs are only observed at high β_p, and in the absence of any enhanced MHD turbulence. Pedestal collisionality in grassy ELMy H-modes in JT-60U is quite low ($0.1 \lesssim \nu_e^* \lesssim 0.3$), although low collisionality is not identified as a condition for access. In both regimes, the suppression of Type I ELMs does not lead to significant changes of the global particle confinement or impurity transport, indicating that additional transport mechanisms replace the bursty losses of Type I ELMs.

Simultaneous high confinement and density are routinely achieved in steady-state conditions for $\sim 20\tau_E$ in JET with highly shaped plasmas. The normalized parameters required for the $Q = 10$ inductive operation of ITER, namely $H_{98} \sim 1$, density $>85\%n_{\rm GR}$ and $\beta_N \sim 2$ with $q_{95} \sim$ 3–3.6, are obtained in lower SN plasmas, with average triangularity at the separatrix of $\delta \sim$ 0.4–0.5. These plasmas are characterized by an external transport barrier and Type I ELMs. As described in (Saibene *et al* 2002), increasing the pedestal density $n_{\rm ped}$ above a critical value (typically $n_{\rm ped} >$ 70–80%$n_{\rm GR}$) at constant plasma parameters, results in a reduction of the Type I ELM frequency $f_{\rm ELM}$ down to a few hertz, while Type I ELM prompt energy losses do not increase, or even decrease, compared to those of Type I ELMs of the same frequency but at lower density. This change in the Type I ELM behaviour occurs at constant (or slightly increased) plasma confinement (H_{98} is no longer decreasing with density (Saibene *et al* 2001)) and pedestal pressure, up to $n_{\rm ped} \sim n_{\rm GR}$. Global power balance shows that the reduction in $f_{\rm ELM}$ is accompanied by enhanced energy and particle losses between ELMs, attributed to the presence of an additional edge loss mechanism, identified, by analogy with ASDEX Upgrade, as Type II ELMs. Type II ELMs in JET are characterized by specific and reproducible changes in the spectrum of MHD fluctuations, namely by an increase in broadband fluctuations in the 10–40 kHz range (Saibene *et al* 2002) compared to similar plasmas having pure Type I ELMs. These broadband fluctuations, localized at the plasma edge, are identified as strong wash board (WB) modes (Perez *et al* 2004). WB modes are regularly observed in H-mode plasmas in JET. They are continuous bands of fluctuating MHD, rotating in the electron diamagnetic drift direction (i.e. they are counter-rotating with respect to the main plasma toroidal rotation). Typical toroidal n numbers are -1 to -8. The correlation between the intensity (and frequency) of WB activity and the build-up of the pedestal temperature indicates that WB modes affect the evolution of the H-mode pedestal and may be responsible for enhanced energy transport across the separatrix. The observed increase of WB mode intensity with fuelling and high pedestal density (favoured by high δ) may indicate that the growth of these modes is favoured by high pedestal collisionality, although no clear collisionality scaling has been found. In fact, in Type II ELM phases, WB mode activity is more intense and has constant frequency, while the temperature $T_{\rm ped}$ at the top of the pedestal reaches saturation. The rate of increase of $n_{\rm ped}$ is reduced, but does not go to zero, eventually leading to a stability limit and a Type I ELM.

As reported in (Saibene *et al* 2002), initial experiments to improve the mixed Type I–II regime up to total Type I ELM suppression were not successful in JET; in particular, attempts to increase the plasma edge density even further lead to a transition to Type III ELMs and reduced plasma confinement.

This paper analyses the key experimental conditions required in JET for accessing high-confinement, small ELM H-mode conditions, as well as trying to identify physics mechanisms that may be responsible for the change in the pedestal dynamics. The role of proximity to QDN, identified in the ASDEX Upgrade experiments, as well as of q_{95}, are analysed for the JET cases, and their possible influence on pedestal MHD stability discussed. Steady-state Type II ELMs are obtained in ASDEX Upgrade at pedestal collisionalities well above the predicted values for the $Q = 10$ inductive reference scenario of ITER ($\nu_e^* \sim 0.07$). Similarly, the pedestal collisionality of mixed Type I–II H-modes in JET is quite high, with $\nu_e^* \sim$ 0.5–1. These observations indicate that the physics mechanism responsible for the quasi-continuum losses replacing Type I ELMs may require a high collisionality/low temperature plasma edge (for instance, high ν_e^* could reduce the edge bootstrap current and affect MHD stability, or resistive MHD could play a role, etc), making it impossible to extrapolate these regimes to ITER conditions. On the other hand, high confinement H-modes, with simultaneous small ELMs and high pedestal pressure have been obtained in JET, in a scenario similar to the grassy ELMy H-modes of JT-60U. As in JT-60U, high β_p is required in JET to obtain this regime. As will be shown, the pedestal collisionality of JET grassy ELMy H-modes is reduced compared to that of Type II H-modes, although it is still higher than in JT-60U at similar β_p and the magnetic spectra are significantly different from Type II H-modes.

Table 1. Summary of magnetic geometry and main plasma parameters of the configurations used in the small ELM experiments described in this paper. All SN configurations have the second x-point outside the vacuum chamber, while for QDN configurations the second x-point is inside. These magnetic configurations are further described in terms of Δ_{sep}, the distance (mapped to the outer midplane) between the first and second separatrix. Several variants of the QDN configuration were used in the experiments, such as variations of Δ_{sep} in QDN1 (Δ_{sep} from $\sim$2 cm to $\lesssim$1 cm), reduced δ and κ for QDN-sim and small modification of the divertor strike point position in the high-l_i/high-β case. Note that $\Delta_{sep} \gtrsim 4$ cm for the SN configurations. $*$ = elongation and average traingularity varied in the scan of the first-to-second separatrix distance.

Configurations	Name	I_p (MA)	B_T (T)	q_{95}	κ_{sep}	$\delta_{sep,average}$
SN	HT3	2.5	2.7–3.4	3.6–4.6	1.74	0.42
QDN	QDN1*	2.5–2.1–1.9	2.7	3–3.7–4.1	1.75–1.9*	0.43–0.50*
QDN	QDN-sim	0.87–(1.2–1.5)	1.17–(1.6–2.0)	4.1	1.7	0.35
QDN	high-l_i/high-β_p	1.5 $\rightarrow$ 1.2	2.7	4.8 $\rightarrow$ 6.9	1.62	0.45
SN	low-l_i/high-β_p	1.2	2.7	6–7	1.62	0.45

1.1. The experiments

As outlined in section 1, this paper presents the results of a series of experiments investigating the behaviour of the plasma pedestal and ELMs in high density/high confinement ELMy H-modes in JET, and the access to small ELM regimes. The full set of H-mode diagnostics available in JET was exploited in these experiments, including fast ECE, magnetics and reflectometry measurements. Profile data were acquired with core and edge charge-exchange diagnostics for T_i measurements, edge and core LIDAR for n_e and T_e data. For a detailed description of the characteristics of the diagnostic used for H-mode physics studies in JET, please refer to Saibene *et al* (2002).

The investigation focuses on three main sets of experiments using several different plasma configurations that are briefly described in table 1, together with some general parameters covered in the study. The following experiments were carried out.

(1) The exploration of the effects of the plasma boundary magnetic geometry (triangularity δ, as well as proximity to double null) and of q_{95} on global confinement, pedestal parameters, ELM type and losses. These experiments were aimed at obtaining a steady-state Type II ELM regime for typical JET H-mode plasma parameters, and at the study of access conditions by direct comparison of pedestal and ELM characteristics in high δ SN and QDN plasmas, under similar experimental conditions. The experiments were carried out mainly in two configurations: a SN configuration named HT3 and a high δ, high elongation, QDN configuration called QDN1 (see table 1). Additional heating was a combination of dominant NB injection (13–16 MW), with the addition of 2–3 MW of central ICRH (H minority heating). In QDN, machine safety considerations (in particular, issues of plasma vertical stability to large Type I ELMs in highly elongated plasmas (Sartori *et al* 2005)) restricted operations to high density, where the Type I ELM size is reduced, and fast vertical excursions of the plasma more easily controlled. The results of these experiments are presented in section 2.

(2) The investigation of the role of proximity to double null for achieving Type II ELM H-modes, in a dimensionless identity experiment with ASDEX Upgrade. For this experiment, the QDN1 configuration was adapted to match the average δ and κ and Δ_{sep} of Type II ELM discharges in ASDEX Upgrade. The plasma current and field were scaled to obtain a dimensionless identity with our model ASDEX Upgrade Type II H-mode plasma. This identity, for JET, is a plasma at 0.87 MA/1.17 T, with average $\delta \sim 0.44$ and a QDN configuration (QDN-sim, table 1) with $\Delta_{sep} \sim 1$ cm, and this was kept fixed for this experiment. As in ASDEX Upgrade, neutral beams were the dominant additional heating (up to $\sim$4 MW), with small amounts of ICRH (H minority heating, central resonance, $\lesssim$1 MW). In this geometry, the plasma current and magnetic field were increased at constant q_{95} to investigate the effect of varying pedestal parameters and H-mode threshold on Type II ELM access. The results of these experiments are discussed in section 2.4.

(3) The study of the effect of β_p on the pedestal and ELM activity (Saibene *et al* 2004), in analogy with JT-60U, where 'grassy ELMs' spontaneously replace Type I ELMs in H-modes, when a threshold value of β_p is exceeded ($\beta_p \gtrsim 1.6$). In JT-60U, high q_{95} and δ are also required to access the grassy ELM regime, but a trade-off has been identified experimentally between the value of the safely factor and shape (Kamada *et al* 2002). In contrast to the JET/ASDEX Upgrade identity, no attempt was made in these experiments to obtain a dimensionless match in JET of the JT-60U plasma parameters, with the exception of β_p. In particular, the experiments in JET were carried out in plasmas with a fully penetrated current profile, no ITB and QDN magnetic geometry. β_p was increased in steps from 1.1 to 1.9, by increasing the input power (combined NB and H minority central ICRH) and, at the maximum input power, reducing the plasma current at fixed field. These discharges will be referred to as 'high-l_i' H-modes. The results from these experiments are described in section 3 and compared to standard ELMy H-modes at low β_p ($\beta_p < 1$) and to a series of discharges at low l_i but same current and field, 1.2 MA/2.7 T, and with β_p in the same range $\sim$1.1–1.9 as the high-l_i H-modes. The low-l_i H-modes used current profile control to obtain plasmas with $q_0 > 2$ and a broad current profile ($l_i \sim 0.85$). The discharges are standard lower SN, with the same δ, κ and similar q_{95} as the QDN high β_p described above.

2. Comparison of high-δ SN and QDN H-modes for variable q_{95}

This section compares the results of the studies of H-mode characteristics and ELM behaviour of highly shaped SN and QDN plasmas in JET. In particular, section 2.1 analyses pedestal and ELM characteristics, as well as global confinement, of the HT3 and QDN1 configurations. Most of the experiments were carried out at 2.5 MA/2.7 T, with $\beta_N \sim$ 1.8–2.0. As shown in table 1, this combination of

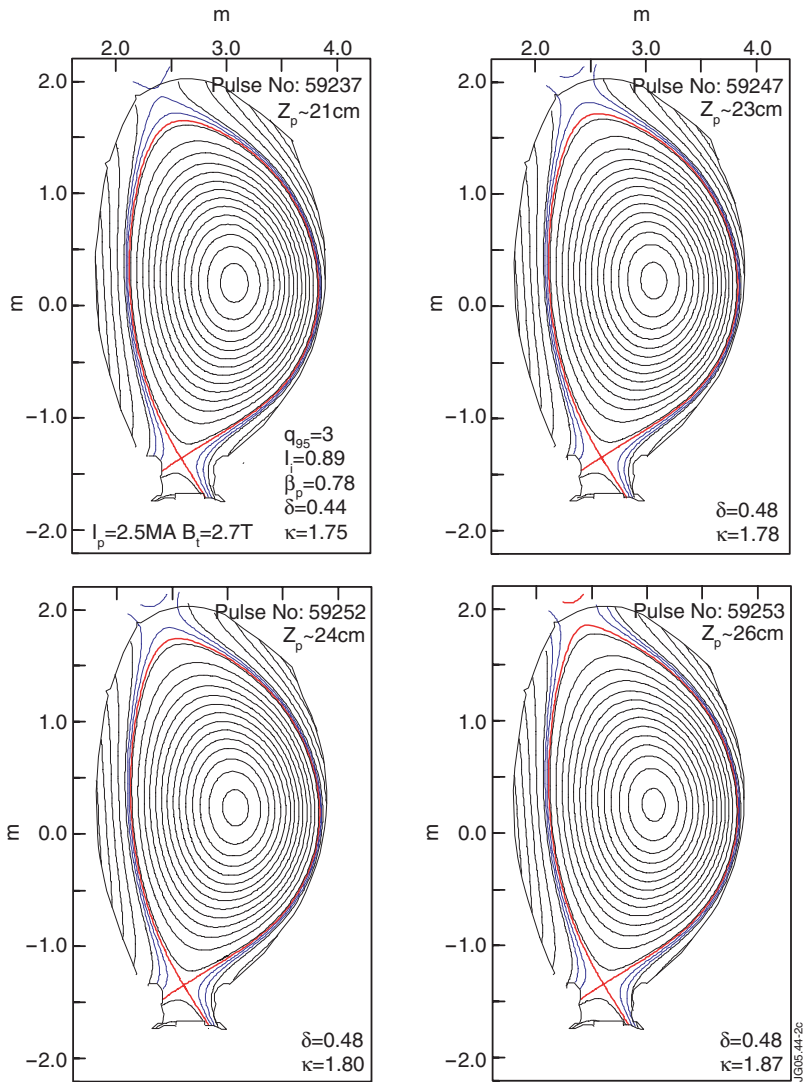

Figure 1. Equilibrium reconstruction of four plasma discharges used for the QDN proximity studies. The variation of Δ_{sep} from ~ 2 cm to < 1 cm is achieved by moving the plasma vertically upwards (as indicated by the variation of the plasma centroid position Z_p shown for each case). The blue lines (dotted in the b/w version) are the 1 cm and 2 cm midplane flux surfaces.

current and field correspond to edge safety factors between 3 and 3.6, depending on the plasma minor radius of the different configurations; a series of experiments was also carried out to study the effect of the edge safety factor on Type II ELM access both in SN and QDN, varying q_{95} from 3.6 $\rightarrow$ 4.6 and 3 $\rightarrow$ 4.1, respectively. In contrast to earlier experiments (see, for instance Saibene *et al* (2002)), the variation of the safety factor in SN was achieved by varying the toroidal field at constant plasma current. This choice was motivated by the observation of the $\sim I_P^2$ dependence of the pedestal pressure of JET ELMy H-modes (not strongly dependent on q_{95}, for the range of q_{95} investigated in this paper (Loarte *et al* 2004)). These conditions were chosen because it was thought that any change in the ELM behaviour with q would be easier to interpret. The observations related to the onset of Type II ELMs for these experiments are summarized in sections 2.2 and 2.3, while the results of the JET/ASDEX Upgrade dimensionless identity with a QDN plasma shape are described in section 2.4.

2.1. Pedestal parameters and confinement

2.1.1. SN versus double null. The role of the second null in determining the onset of Type II ELMs was investigated by varying the first-to-second separatrix distance Δ_{sep}, moving the plasma vertically upwards in 4 fine steps in four separate discharges. The equilibria corresponding to each discharge/Δ_{sep} value are shown in figure 1, while the poloidal distribution of radiation for each case is shown in figure 2. While the stronger radiation emission is in the lower x-point region for $\Delta_{sep} \geqq 2$ cm, radiation from the upper x-point region increases as the plasma is moved upwards and Δ_{sep} reduced. For $\Delta_{sep} < 1$ cm, the upper x-point region dominates the radiation emission. On the other hand, power balance calculations carried out using the divertor thermocouples system show that the power flow is still predominantly conducted to the lower x-point region, even for the minimum Δ_{sep} ($\sim$35% maximum power deficit to the lower divertor). This indicates that, although the recycling pattern

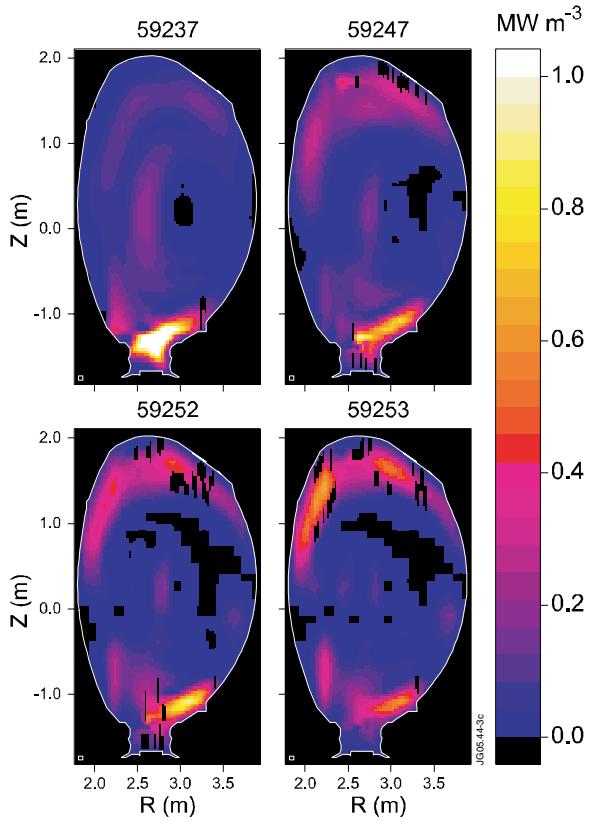

Figure 2. Tomographic reconstruction of the poloidal distribution of the radiation emission for each of the four plasmas shown in figure 1.

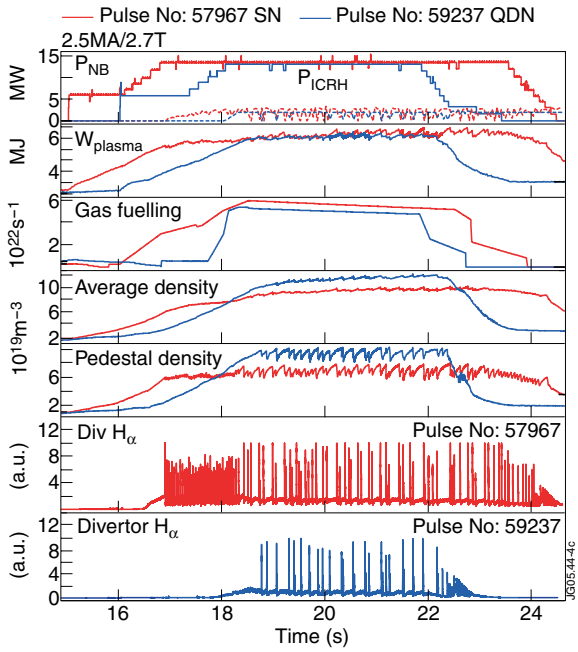

Figure 3. Selected time traces of the SN HT3 pulse #57987 (red traces, full lines in the b/w version) and of the QDN QDN1 pulse #59237 (blue traces, dotted in the b/w version). Pulse #59237 is the QDN pulse that reached the highest plasma confinement, and has comparable stored energy to similar SN pulses, and to #57987 in particular. $I_p = 2.5$ MA and $B_T = 2.7$ T for both pulses, with $q_{95} = 3.6$ and 3, respectively. Both #57987 ($18 \rightarrow 23$ s) and #59237 ($19 \rightarrow 22$ s) are in the mixed Type I–II regime. The traces in the graph are, from top to bottom: NB ($P_{\rm NB}$, MW) and ICRH ($P_{\rm ICRH}$, MW) input powers; plasma stored energy ($W_{\rm plasma}$, MJ); gas fuelling rate (10^{22} atoms s^{-1}); plasma average density (10^{19} m^{-3}); pedestal density (10^{19} m^{-3}) and, in the last two boxes, divertor H_α emission.

changes when reducing $\Delta_{\rm sep}$, the active divertor is still the lower one, even for the minimum $\Delta_{\rm sep}$.

It is found that, at 2.5 MA and $q_{95} \sim 3$–3.6, the plasma enters the mixed Type I–II regime, for both SN and QDN configurations for $n_{\rm ped} \gtrsim 70$–$80\% n_{\rm GR}$, with typical Type I ELM frequency $f_{\rm ELM}$ of 6–10 Hz, compared to ∼15–20 Hz of the unfuelled, lower $n_{\rm ped}$ cases. The lower $f_{\rm ELM}$ (∼6 Hz) is measured for QDN plasmas, for otherwise similar plasma conditions. The overall similarity of the pedestal and ELM behaviour for SN and QDN plasmas in JET is illustrated in figure 3, by comparing selected time traces of #57987 (SN HT3) and of #59237 (QDN QDN1), both at 2.5 MA/2.7 T. Pulse #59237 has $\Delta_{\rm sep} \sim 2$ cm, and it was selected because it produced the best performance, in terms of both core and pedestal parameters, of the series of QDN1 where $\Delta_{\rm sep}$ was varied. The two discharges have almost identical input power and similar gas fuelling: both reach extremely high densities with a mixed Type I–II H-mode edge. Figure 3 also exemplifies some of the differences between SN and QDN H-mode behaviour: for the same external fuelling; the QDN plasma reaches higher absolute densities on average and in the pedestal, although $n_{\rm ped}/n_{\rm GR}$ is similar for the two discharges (∼ 78% for SN and 83% for QDN). A crude estimate of ELM particle losses for the two cases in figure 3 shows that, in spite of the reduced Type I ELM frequency, Type I ELM particle losses for the QDN #59237 are approximately 90% of those of #57987 (SN), indicating that it is unlikely that the higher plasma density obtained in QDN is just due to a reduction of ELM particle losses. In general, approaching a double null configuration (by reducing $\Delta_{\rm sep}$) reduces, by up to a factor of ∼ 2, the amount of external fuelling required to reach a certain steady-state $n_{\rm ped}$ compared to the HT3 plasmas, consistent with increased particle recycling from the upper x-point region and, possibly, deeper neutral penetration.

The reduction of $\Delta_{\rm sep}$ from ∼2 cm to quasi-pure double null geometry, while the plasma pedestal is in the mixed Type I–II regime, does not result in the suppression of Type I ELMs, but rather in a reduction of $p_{\rm ped}$ and transitions to Type III ELMs. Although repetitive plasma discharges were successfully used to condition the upper x-point target, the lack of active pumping in the upper divertor region may nonetheless affect the plasma response to external fuelling and possibly the observed ELM behaviour. An increase of the L → H transition power with decreasing $\Delta_{\rm sep}$ could also be a reason for the occurrence of Type III ELMs when approaching a double null configuration, but no study of the variation of the L → H transition power with $\Delta_{\rm sep}$ was carried out in these experiments. The typical input power used in the QDN discharges with $q_{95} = 3$ was $P_{\rm in} \approx 1.5 P_{\rm L\rightarrow H}$, while at higher q_{95}, this margin was increased to $P_{\rm in} \approx 2.3 P_{\rm L\rightarrow H}$. In the absence of more evidence, it is not possible to establish if a possible increase of the L → H transition power may have affected the ELM behaviour of the QDN plasmas although, at least for $q_{95} \geqslant 3.6$, the margin of the input power over the threshold power was large enough to leave ample margin in the Type I regime (Sartori *et al* 2002).

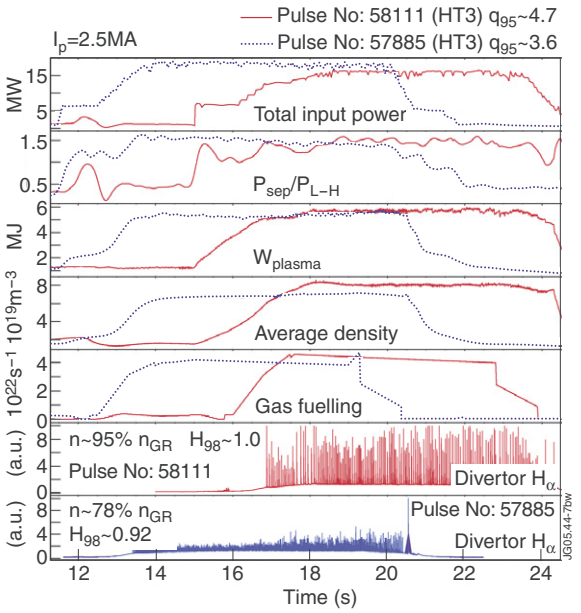

Figure 4. Selected time traces for 2 SN HT3 H-modes at 2.5 MA: #57885 (red, full line in the b/w version), with $B_T = 2.7$ T and $q_{95} \sim 3.6$ and #58111 (blue, dotted line in the b/w version), with $B_T = 3.4$ T and $q_{95} \sim 4.7$. The time traces are, from top to bottom: total input power ($P_{\rm tot}$, MW), ratio of the power across the separatrix $P_{\rm sep}$ to the H-mode power threshold $P_{\rm L-H}$ (Ryter *et al* 2001) ($P_{\rm sep} = P_{\rm tot} - P_{\rm rad} - {\rm d}W/{\rm d}t$), plasma stored energy ($W_{\rm plasma}$, MJ), plasma average density (10^{19} m^{-3}), gas fuelling (10^{22} atoms s^{-1}) and, last two boxes, divertor H_α emission, in arbitrary units.

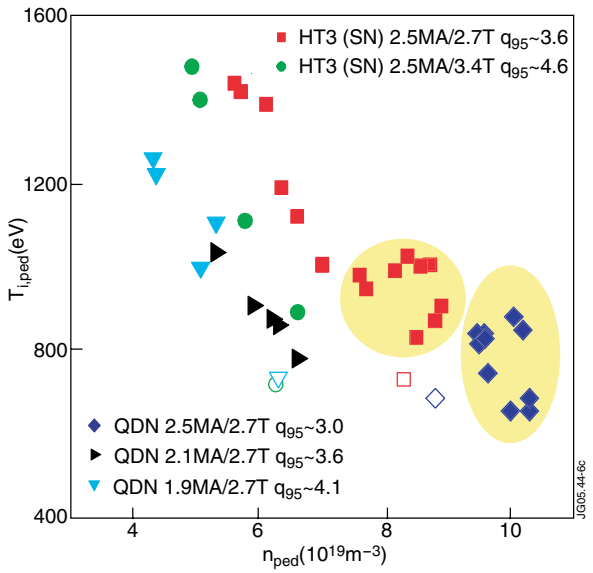

Figure 5. n_e–T_i diagram for the top of the pedestal for both HT3 and QDN1 H-modes, including the q_{95} scans. T_i (from the edge charge-exchange spectroscopy system) is used instead of T_e because the latter is not available for all discharges due to ECE emission cut-off at high pedestal densities. The yellow shaded areas identify points with mixed Type I–II ELMs.

2.1.2. Variations of q_{95}. Experimental evidence from ASDEX Upgrade (Stober *et al* 2001) shows that a high edge safety factor ($q_{95} \gtrsim 4$) facilitates the access to steady-state Type II regimes. This was tested in the JET experiments, where q_{95} was increased in both SN and QDN configurations, and a gas scan and proximity to double null scan carried out. In the case of the SN, q_{95} was increased to 4.6 at constant I_p (experiments where q_{95} was increased at constant B_T for SN reported in Saibene *et al* (2002)), while for QDN1, due to limitations on the allowable power load to the upper x-point region, q_{95} was raised from 3.1 to 3.6 and then to 4.1 by decreasing I_p (i.e. without increasing the L–H power threshold, and therefore the required input power). As an example, time traces of two SN HT3 plasmas are compared in figure 4: for the same plasma current and external fuelling, and with equivalent input power (normalized to the L → H transition power), the plasma with higher q_{95} (pulse 58111) has a reduced confinement enhancement factor, reaches a lower density and has much more frequent Type I ELMs ($f_{\rm ELM}(58111) \sim 50$–$70$ Hz while $f_{\rm ELM}(57885) \sim 25$ Hz). Figure 4 is an illustration of a general result: increasing q_{95}, for both SN and QDN results in a strong increase in the ELM frequency (by a factor of 2–3). Note also that the reduction in pedestal pressure with q_{95} is particularly severe at high density, while the pedestal pressure of the low density, unfuelled discharges, is similar at low and high q_{95} (Loarte *et al* 2004, Sartori *et al* 2004a).

The behaviour of the pedestal parameters is illustrated in figure 5, showing the edge operational diagram n_e–T_i for density scans in SN HT3 and QDN QDN1 configurations, for all the values of q_{95} explored. Note that the data for QDN at $q = 3$ (2.5 MA–2.7 T) in the Type I ELM regime are missing, because low density operation in that configuration and at that current was deemed unsafe: the QDN1 configuration has a very high vertical instability growth rate, and it is susceptible to disruptions due to the loss of vertical position control caused by large Type I ELM disturbances. The results summarized in figure 5 are similar and consistent with those reported in Saibene *et al* (2002), where a q scan was carried out in SN by decreasing I_p at constant B_T. As the SN data in figure 5 clearly show, the maximum pedestal (and core) density achievable at $q_{95} = 4.6$ before the Type I–III ELM transition is substantially reduced compared to the lower q_{95} cases, from 90% down to 60–70%$n_{\rm GR}$. Concentrating again on the SN data (because they are more complete), the reduction of the maximum density achievable in a pure Type I ELM regime with q_{95} is consistent with a $Bq^{-5/4}$scaling, that describes other JET data quite well (Chankin and Saibene 1999, Sartori *et al* 2004b). This scaling is based on the identifications of three key dimensionless parameters for the description of the H-mode edge operational space: a dimensionless critical pressure gradient representing the ideal ballooning instability, for the Type I ELM boundary; collisionality as representative of resistive ballooning instabilities for the onset of Type III ELMs and a dimensionless critical temperature, representing the L → H transition boundary. Scaling expression for critical transition points, such as the critical density for the Type I → Type III transition or the H-mode density limit, are then determined by fixing pairs of these dimensionless parameters. This study on access conditions for small ELM regimes is a step towards understanding the operational space for those ELMs, by trying to identify critical access parameters, as well as checking the consistency of experimental observations with other H-mode boundaries, such as the Type I → Type III

transition and the L → H threshold boundary (see also section 2.4).

The high confinement at high density obtained in the SN HT3 at $q_{95} = 3.6$ corresponds to a clamping of T_{ped} for increasing density, i.e. to an effective increase of the pedestal pressure with density and to the onset of mixed Type I–II ELMs. This is the case also for the QDN1 at low q_{95}, although T_{ped} is somewhat reduced compared to the SN plasmas, as is H_{98}, but it is not observed at higher q_{95}. Increasing q in both SN and QDN results in a reduced pedestal pressure as well as in a transition to Type III ELMs at lower n_{ped}, compared to plasmas at the same I_p but with $q_{95} \sim 3$–3.6. As mentioned in section 1, the onset of mixed Type I–II ELMs is characterized by an anomaly in the frequency of Type I ELMs that, instead of increasing for increasing n_{ped} (at constant power across the separatrix), starts to decrease. In low q SN H-modes, the onset of mixed Type I–II ELMs occurs at $n_{ped} \sim 70\% n_{GR}$. In the case of the $q_{95} = 4.6$ H-modes, the Type I ELM frequency starts to decrease at $n_{ped} \sim 60\% n_{GR}$, possibly indicating a lower density onset for Type II ELMs than low q H-modes. On the other hand, increasing the fuelling further does not increase the pedestal density significantly, but triggers a transition to Type III ELMs. Although the variation of the maximum n_{ped} achievable before the transition to Type III ELMs is consistent with previous scalings, it is not clear why mixed Type I–II ELMs are obtained in JET at low q, but not at high q. From the observation that Type II ELMs are obtained at high collisionality, one could interpret the access to Type II ELMs as being bound between the Type I–III ELM transition and some critical collisionality value. The analysis of the SN data does not entirely support this idea: pedestal collisionalities of the highest density plasma with Type I ELMs are comparable at high and low q_{95} ($\nu^* \sim 0.4$ for $q_{95} = 3.6$ and $\nu^* \sim 0.5$ for $q_{95} = 4.6$). This would indicate that, although Type II ELMs are observed only at high collisionality, access to Type II ELM pedestal is not determined by a simple collisionality threshold.

QDN plasmas at high q_{95} show a similar behaviour to the SN discharges, although the minimum density for the onset of mixed Type I–II ELMs could not be determined because of the operational constraints mentioned above. At higher q, access to mixed Type I–II ELM regime is essentially precluded, with the maximum pedestal density being limited by the transition to Type III ELMs, taking place at lower n_{ped}.

The behaviour of the global plasma confinement is consistent with the picture given by the pedestal parameters. The confinement enhancement factor H_{98} for SN HT3 at 2.5 MA/2.7 T and that of QDN1 at same I_p and B_T are compared in figure 6. Each point represents a plasma discharge and the shaded areas indicate discharges in the mixed Type I–II regime. The normalized confinement of the QDN plasmas is 10% to 20% lower than the reference HT3, for the same I_p and normalized n_{ped}. The lowest H_{98} values in QDN1 shape correspond to plasmas with the lowest Δ_{sep}, i.e. closest to pure double null. For both configurations, the core density profiles are weakly peaked ($n_{core}/n_{ped} \sim 1.2$), while QDN1 plasmas systematically reach higher absolute densities. The reduction of the normalized confinement mentioned above is not entirely accounted for by the predicted positive density dependence of H_{98} ($H_{98} \propto n^{+0.4}$ in the scaling) not found in the data, but also reflects the somewhat reduced plasma energy content compared to equivalent SN plasmas.

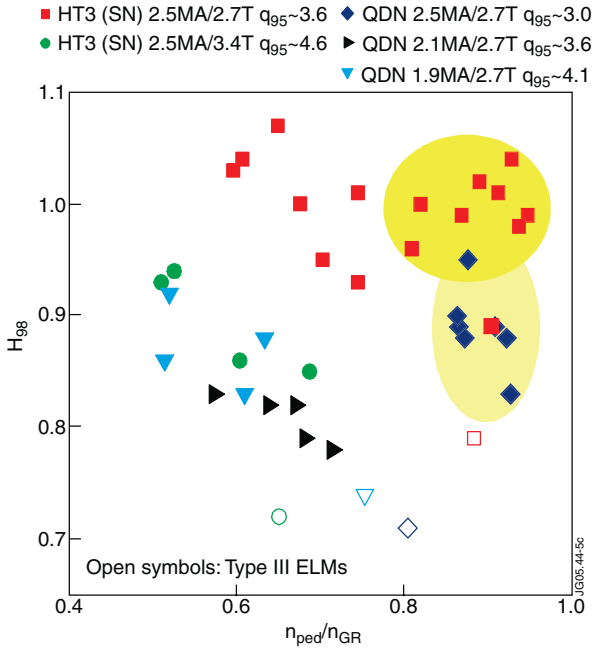

Figure 6. Confinement enhancement factor H_{98} as a function of normalized pedestal density n_{ped}/n_{GR}, for both HT3 and QDN1 plasmas, including the q_{95} scans (same discharges and symbols as figure 5).

The dependence of the global plasma confinement on q_{95} is not well understood: the 'optimal' q value for access to the mixed Type I–II regime (i.e. to high density and high confinement) depends on the plasma configuration: as figure 6 shows, the best n–H_{98} combination is achieved in HT3 SN for $q_{95} = 3.6$ (Sartori *et al* 2004a) while, increasing q_{95} above 3, already results in reduced performance in the QDN configuration.

2.2. *Type II ELM characterization*

An interpretation of the change in ELM behaviour at high density (and increased inter-ELM losses; see section 2.3) comes from the analysis of magnetic and density fluctuations. As already shown in (Saibene *et al* 2002), Type II ELMs in JET are accompanied by an increase of the intensity of broadband magnetic fluctuations at low frequency, associated with the changes in the pedestal and ELM behaviour described above. These broadband MHD events are called in JET wash board modes, or WB modes. As studied in detail in Perez *et al* (2004), there are strong indications that the presence of these modes has a 'regulating' effect on the pedestal pressure and may be responsible for enhanced transport across the separatrix. In other words, increasing the intensity of WB modes (ubiquitous in the edge of Type I ELMy H-modes in JET (Smeulders *et al* 1999)) may be associated with enhanced energy and particle losses between Type I ELMs (Perez *et al* 2004, Koslowski *et al* 2003).

Figure 7 compares the MHD fluctuation intensity for four representative discharges in this study: two SN (HT3) at $q_{95} = 3.6$ with Type I and mixed Type I–II ELMs (#57897 and #57987, figure 7(*a*)), SN versus QDN1, at the same I_p and B_T, both with mixed Type I–II ELMs (#57987 and

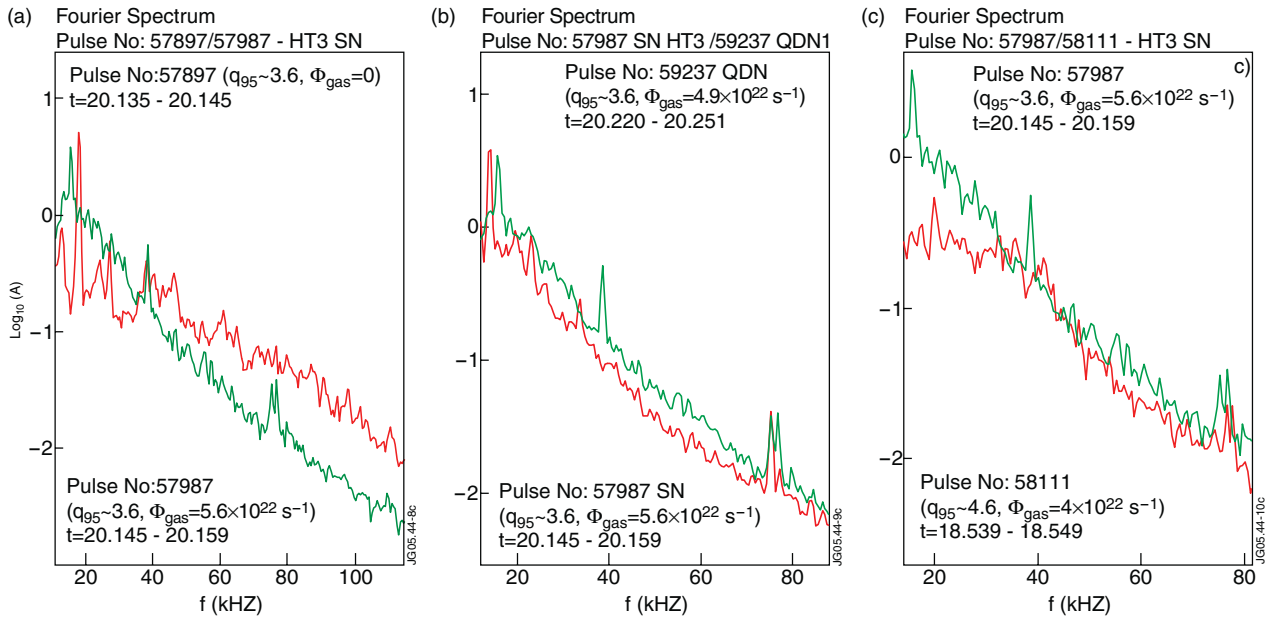

Figure 7. Comparison of the intensity of MHD fluctuations for three pairs of pulses. Left, (*a*): HT3 at low q Type I (red) and Type II (green); middle, (*b*): SN HT3 (red) versus QDN1 (green) at 2.5 MA/2.7 T, Type II phases; and last to the right (*c*) HT3 at low (green) and high q_{95} (red). Note that the high frequency part of the spectrum is similar for both q_{95}, but the MHD fluctuations of the high q_{95} lack the enhanced activity at low frequency, typical of Type II ELM phases. The red traces are full lines and the green traces are dotted lines in the b/w version of the paper.

#59237, figure 7(*b*) and time traces in figure 3) and last, low q_{95} versus high q_{95} in SN at high n (#57987 and #58111, figure 7(*c*)). Figure 7(*a*) illustrates the typical change in MHD activity in the periods between Type I ELMs, at low and high pedestal density (pulses 57897 and 57987) and the appearance of Type II ELMs 'signature'. The intensity of the MHD activity decreases at high frequency (>40 kHz), while it is enhanced around the 20 kHz level (±10 kz). This is clearly visible in the spectrograms for these two same discharges (figures 8(*a*) and (*b*)), which also show the reduction in the Type I ELM frequency in the presence of the enhanced inter-ELM MHD activity. Figure 7(*b*) shows that the WB mode signature for mixed Type I–II ELMs in SN and QDN is quite similar, with the fluctuations having similar intensity and frequency distribution for both configurations (see also figures 8(*b*) and (*c*)). Finally, figure 7(*c*) compares the WB mode intensity for two SN discharges at different q_{95}. Although a reduction of the high frequency MHD fluctuations is observed in both plasmas, at high q_{95} the characteristic intensity enhancement in the 20 kHz range is absent or strongly reduced compared to the low q_{95} cases. The reason for this difference is not, at this moment, understood, but it is obvious that increasing the edge q does not seem to facilitate the access to the mixed Type I–II regime in JET, and even less an opening to total Type I ELM suppression and steady Type II ELM H-mode edge. Increasing q_{95} in the QDN configuration leads to similar results as for SN: at $q_{95} = 4.1$ in the QDN1 shape no clear Type II ELM phases are observed for the investigated fuelling rates and Δ_{sep}.

As mentioned above, the new experiments presented in this work confirm the previous analysis of mixed Type I–II ELMy H-mode plasmas in JET, in particular that the presence of enhanced MHD activity between ELMs corresponds to a clamping of the pedestal temperature rise between ELMs. In fact, after the ELM crash, T_{ped} rises on a short time scale, but then remains essentially constant until the next ELM (Saibene *et al* 2002) (n_{ped} does not reach steady state during the Type II ELM phase). Energy and particle losses of Type II ELMs are discussed in more detail in section 2.3.

The behaviour of the density in the pedestal region during Type II ELM phases has been further investigated. Fast (100 kHz) interferometry measurements in the region of the top of the pedestal show that the increased broadband MHD activity corresponds to a similar increase in the density fluctuations, as illustrated in figure 9 for discharges 57897 and 57987, both 2.5 MA/2.7 T, linking the increase of the WB mode intensity not only to a saturation of T_{ped}, but also to increased particle losses between Type I ELMs (see also Koslowski *et al* (2003)).

Density fluctuations were also measured with a multi-channel heterodyne reflectometer, with a maximum cut-off density of $5.1 \times 10^{19}\,\mathrm{m}^{-3}$. Fluctuations were compared at different positions in the pedestal region. It is found that fluctuation levels between ELMs near the separatrix are very similar for pure Type I and for mixed Type I–II plasmas. Density fluctuations were also compared for density cut-off layers in the region of the maximum ∇n region in the pedestal, for both Type I and mixed Type I–II cases. The position of the selected cut-off layer in the pedestal gradient region for both pulses is shown in figure 10. The density profiles in figure 10 are from pulses 59354 and 59355, which were performed as exact repeats of the SN HT3 Type I ELM discharge 57897 and mixed Type I–II discharge 57987, respectively, to obtain high resolution edge density profiles, missing in the original discharges. A lower cut-off density was selected for pulse 57897 than for 57987, to compare the density fluctuation levels in similar relative positions in the gradient region in both

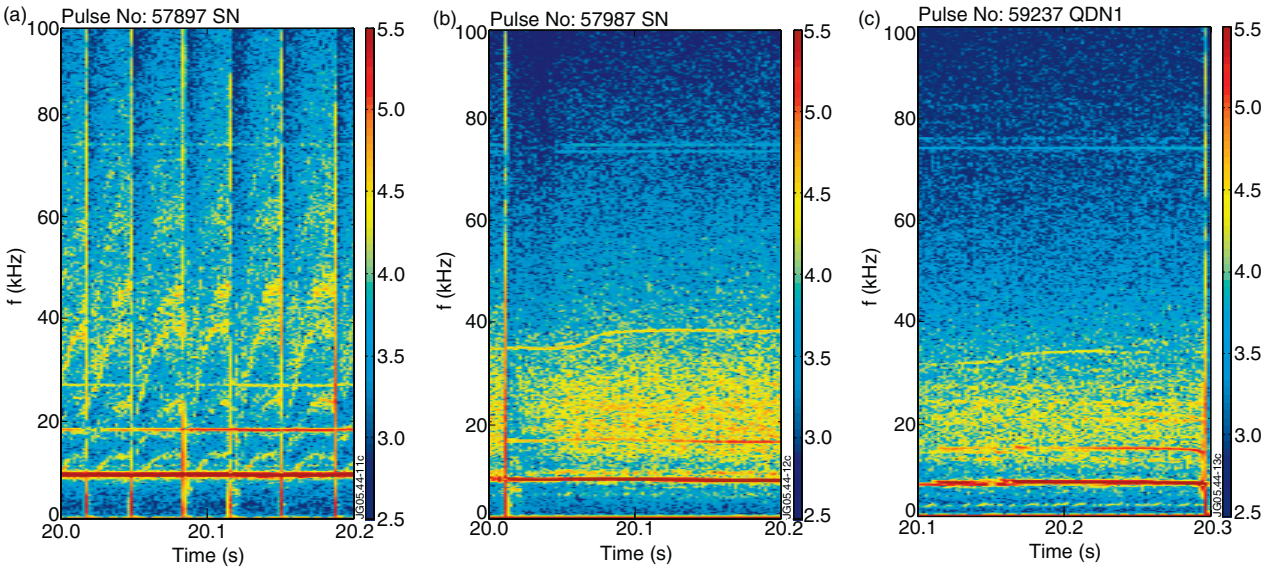

Figure 8. Spectrograms for three of the plasma discharges shown in figure 7. (*a*) SN HT3 2.5 MA/2.7 T Type I (#57897); in the middle, (*b*) SN HT3 2.5 MA/2.7 T with Type II ELMs (#57987) and last, (*c*) QDN1 at 2.5 MA/2.7 T with Type II ELMs (#59237). The intense and narrow vertical bands are Type I ELMs, the horizontal continuous narrow bands with high intensity are correlated to core MHD activity.

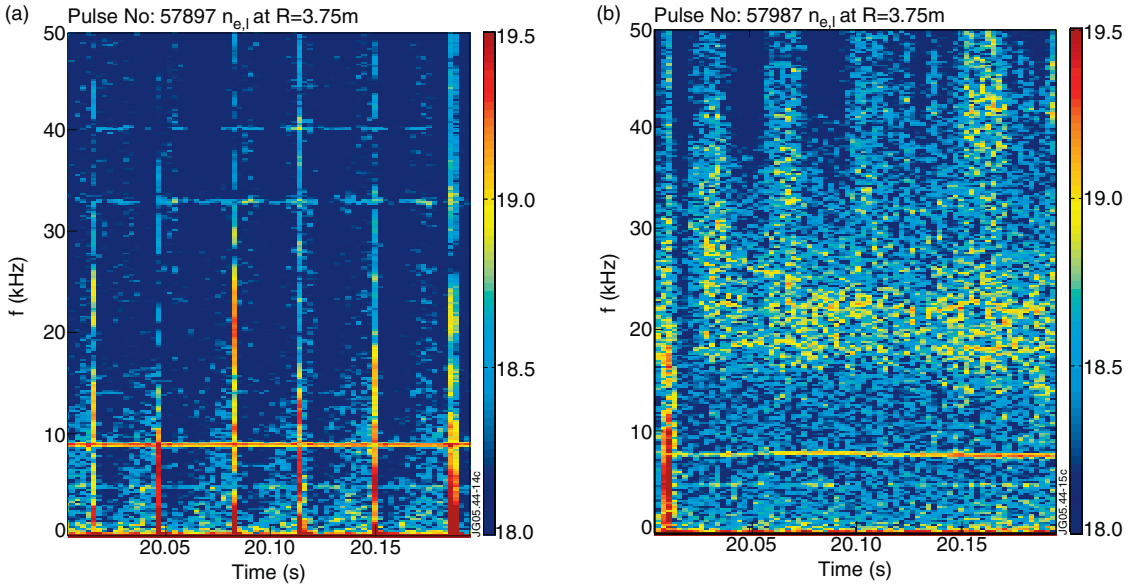

Figure 9. Density fluctuation as measured by fast interferometry in SN, Type I ELMy H-mode (*a*), and mixed Type I–II H-mode (*b*). The same discharges as for figures 8(*a*) and (*b*).

pulses. The corresponding intensity of the density fluctuations between ELMs is shown in figure 11. No significant difference in the frequency distribution of the fluctuations in the steep gradient region of the pedestal is observed, between pure Type I and mixed Type I–II ELMs (both for SN and QDN). In particular, no enhanced broadband fluctuations are observed ∼20 kHz, in contrast to the observation from interferometry. Figure 11 also includes density fluctuation data for the QDN1 discharge #59237, showing a very similar distribution of density fluctuations from the steep gradient region of the pedestal as the other two SN plasmas. The decrease in the absolute intensity of n fluctuations is possibly related to changes of ∇n, and not to changes in turbulence.

The comparison of density fluctuation measurements from interferometry and reflectometry provides some indications on the localization of the edge turbulence. In fact, the interferometer chord used for providing the measurements in figure 9 is vertical and goes across the approximate position of the pedestal top. Also, as discussed earlier, the fluctuation spectrum from these measurements is very similar to that of MHD fluctuations (figures 8(*a*) and (*b*)). On the other hand, the reflectometry measurements in the steep gradient region and close to the separatrix do not show any significant change in the fluctuation spectra between Type I and mixed Type I–II ELMs. These findings suggest that inter-ELM transport in mixed Type I–II H-modes may be enhanced by a perturbation located

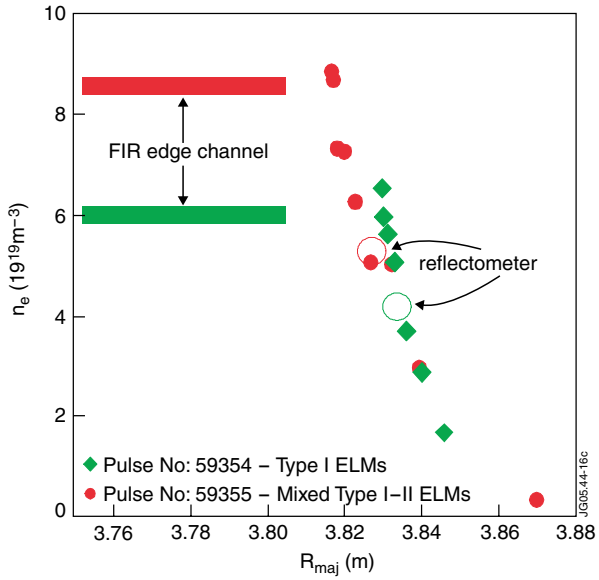

Figure 10. Position of the cut-off density layer in the pedestal gradient region for 59354 (57897, HT3, Type I) and 59355 (57987, HT3, mixed Type I–II).

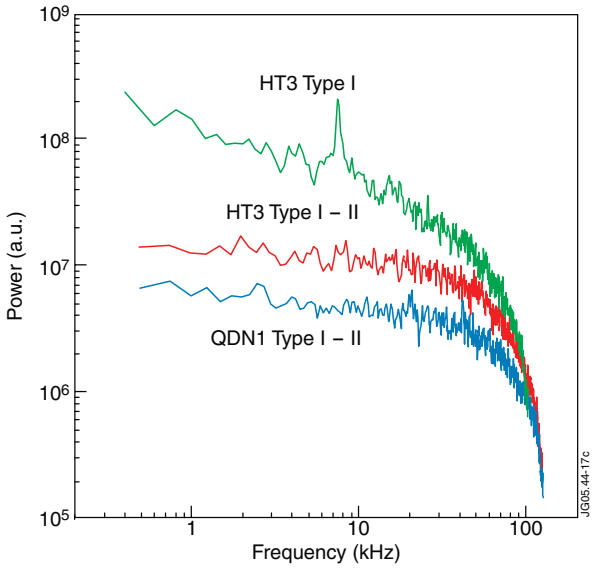

Figure 11. Intensity of density fluctuations for pulses 57897 (green), 57987 (red), and for comparison, the QDN1 2.5 MA/2.7 T, 59237 (blue).

in a very narrow region of the pedestal, probably near the pedestal top.

2.3. Losses in the mixed Type I–II regime

More insight may be gained on the failure to achieve steady Type II ELM regimes in JET, by analysing the changes in the re-heat and particle refuelling rates with ELM type, configuration and q_{95}. The analysis of the rate of rise of the stored energy between Type I ELMs shows that, in general, $\mathrm{d}W/\mathrm{d}t$ is not a constant, even for constant average plasma conditions, with $\mathrm{d}W/\mathrm{d}t$ varying from ELM to ELM, as well as in time, between two ELMs. For the high δ plasmas analysed in this paper, $\mathrm{d}W/\mathrm{d}t$ may vary from ∼10 to near 0 MJ s^{-1} (the stored energy rise between ELMs may reach near-saturation in some low-frequency Type I ELMy H-modes). Nonetheless, it can be shown that a qualitative correlation between $\mathrm{d}W/\mathrm{d}t$ and the intensity of WB mode amplitude exists, in a similar way as reported for the variation in the time evolution of T_{ped} between ELMs (Perez *et al* 2004).

In spite of the ELM-to-ELM variation of $\mathrm{d}W/\mathrm{d}t$, it is found that Type II ELM phases correlate with a reduction of the power carried by Type I ELMs, P_{ELM}. With mixed Type I–II ELMs, the power carried by Type I ELMs is reduced by more than a factor of 2, as exemplified in figure 12, left, comparing the re-heat rate of an HT3 Type I ELMy H-mode with that of a QDN1 with mixed Type I–II ELMs.

The right-hand side plot in figure 12 shows the calculated fraction of power carried by Type I ELMs, P_{ELM} (normalized to P_{sep}) for several 2.5 MA/2.7 T plasmas, with different magnetic configurations. The figure shows clearly that P_{ELM} is reduced from a maximum of 50–60% with Type I ELMs, down to ∼25% in SN plasmas with mixed Type I–II ELMs, and further down to ∼20% for QDN1 with mixed Type I–II edge (or, in other words, ∼80% of the power is exhausted across the separatrix in a quasi-continuous way). Nonetheless, the pedestal pressure is still evolving in the Type II phases, indicating that these additional losses are not sufficient to avoid Type I ELMs completely. In particular, although the edge particle refuelling rate in Type II ELM phases is reduced by a factor ∼2 compared to pure Type I ELM plasmas (figure 13(*a*)), $\mathrm{d}n/\mathrm{d}t$ is still >0. Figure 13(*a*) also shows that the net particle refuelling rate increases with q_{95}, with $\mathrm{d}n/\mathrm{d}t$ at high q_{95} being a factor 1.4–1.8 higher than at lower q_{95}, for similar external gas fuelling. This, not surprisingly, results in a correlation between the higher refuelling rate and Type I ELM frequency (figure 13(*b*)), although the reason why high q_{95} should result in a better effective particle confinement in the edge is not, to date, understood. This change in edge particle transport and the consequent increase of f_{ELM} may partially explain the reduced occurrence of Type II ELM phases at high q_{95} in JET.

2.4. ASDEX Upgrade/JET Type II similarity experiments

The role of plasma magnetic geometry in accessing steady-state Type II ELMy H-modes was further examined in a dimensionless identity experiment between ASDEX Upgrade and JET, as outlined in section 1.1. Two ideas were behind running dimensionless identical plasmas in the two devices: the first was to experimentally test QDN plasmas with the same δ and κ (JET QDN plasmas described in the previous sections are more triangular and elongated than those in ASDEX Upgrade) and also Δ_{sep}; the second was to 'use' the dimensionless identity to discriminate between Type II ELM access being determined by general plasma physics properties (that should be maintained in a dimensionless identity) or by other phenomena, such as atomic physics (changes in recycling and neutral penetration in the upper x-point region, for instance).

The model pulse from ASDEX Upgrade was a 1 MA/2.4 T QDN H-mode plasma ($q_{95} \sim 4.1$), with $H_{98} \sim 0.9$, $T_{\mathrm{ped}} \sim 350$ eV and $n_{\mathrm{ped}} \sim 6.5 \times 10^{19}$ m^{-3} and steady Type II ELMy edge. Applying standard dimensionless identity relations

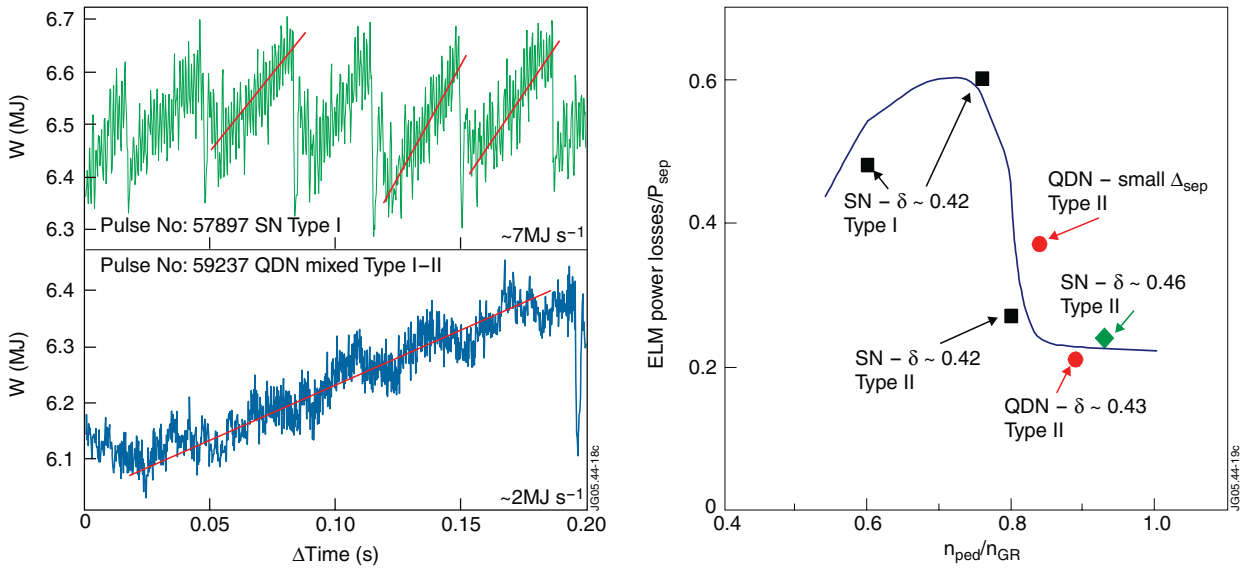

Figure 12. Variation of the re-heating rate between ELMs with ELM type and configuration. Left side: comparison of the time evolution of the plasma stored energy for pulse 57897 (SN HT3, 2.5 MA/2.7 T) with standard Type I ELMs, and that of pulse 59237 (QDN, 2.5 MA/2.7 T) with mixed Type I–II edge. Their magnetic fluctuation spectra are shown in figures 8(*a*) and (*b*). Right side: fraction of the power across the separatrix carried by ELMs compared to the total loss power: this fraction decreases markedly in the mixed Type I–II regime, for both SN and QDN configurations.

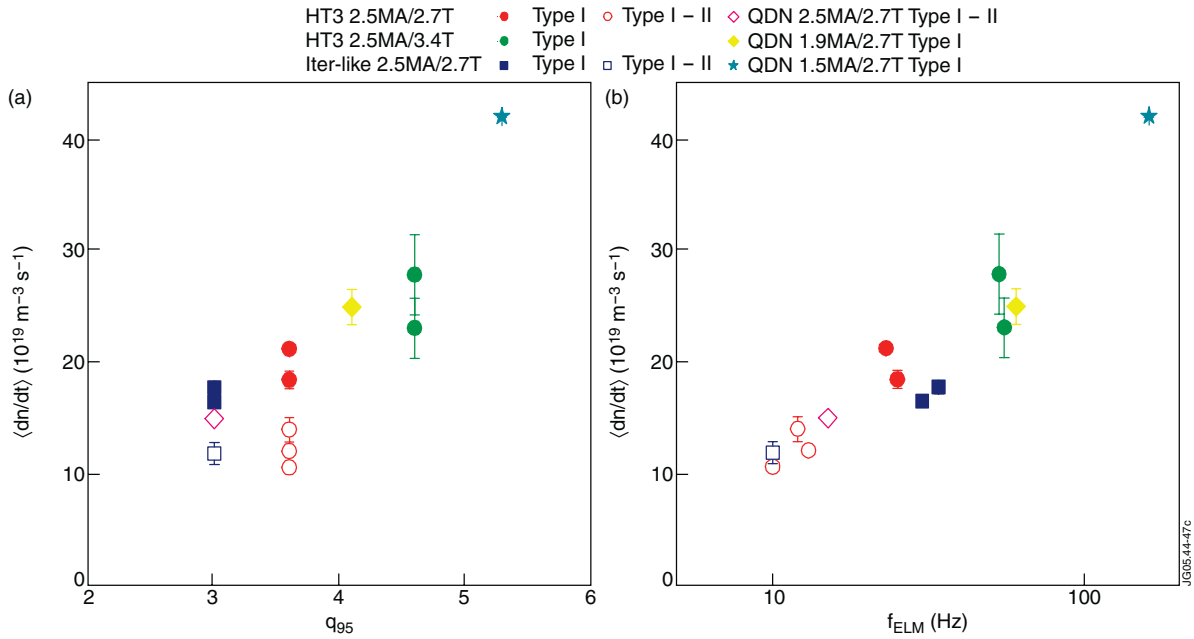

Figure 13. (*a*) Comparison of the average net edge particle refuelling rate between Type I ELMs for SN HT3, QDN, for various q_{95}. (*b*) Average net particle refuelling rate as a function of the Type I ELM frequency, for the same set of data as the plot (*a*) in this figure.

(see, for instance, Cordey *et al* (1996) and references therein), these parameters correspond in JET to 0.87 MA/1.17 T, with expected $T_{\rm ped} \sim 260$ eV and $n_{\rm ped} \sim 2.1 \times 10^{19}$ m^{-3}, to match a pedestal collisionality $\nu^* \sim 2$ and normalized toroidal Larmor radius $\rho^* \sim 4 \times 10^{-3}$. The plasma average δ and κ were also matched, as indicated in table 1 for the configuration QDN-sim.

The results of the experiments in identity conditions may be summarized as follows: long phases of H-mode confinement without Type I ELMs; MHD signature consistent with Type II ELM activity and steady-state pedestal parameters were observed, with $H_{98} \sim 1$ and pedestal densities $n_{\rm ped} \sim 85\% n_{\rm GR}$. The duration of the period at constant pedestal parameters was limited by plasma core instabilities since, at these low input powers, the core plasma suffered from progressive density peaking leading to radiative collapse of the discharge. When either the input power or the plasma current and field were increased (in steps up to 1.5 MA/2.0 T at constant $q_{95} \sim 4.1$), ELM activity typical of standard ELMy H-modes reappeared, and ELM-free phases with constant pedestal parameters were no longer obtained.

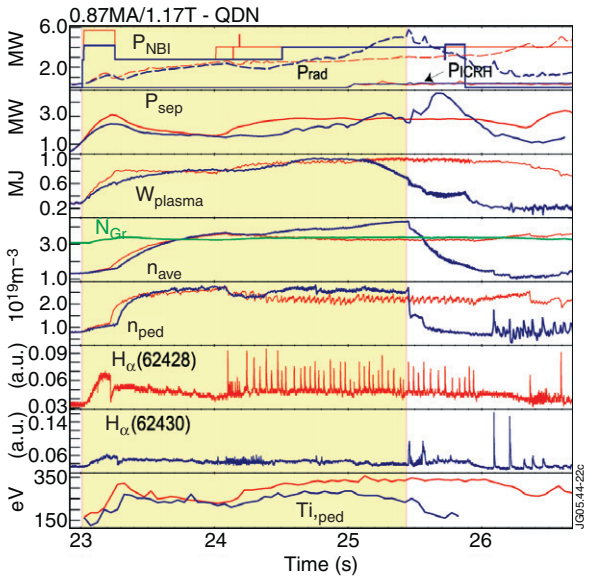

Figure 14. Selected time traces for two pulses of the JET/ASDEX Upgrade identity experiments: in red (dotted in the b/w version), pulse 62428 (Type I ELMs) and in blue (full line in the b/w version), pulse 62430 (Type II ELMs). From top to bottom: NB and ICRH input powers (full lines, $P_{\rm NBI}$ and $P_{\rm ICRH}$, MW) and total radiated power (dashed lines, $P_{\rm rad}$, MW); power across the separatrix, $P_{\rm sep}$, MW); plasma stored energy, $W_{\rm plasma}$ (MJ); line-averaged density, $n_{\rm ave}$ and Greenwald density (green, $n_{\rm GR}$); pedestal density $n_{\rm ped}$, all in units of 10^{19} m^{-3}; divertor H_α (# 62428, a.u.); divertor H_α (# 62430, a.u.) and, finally, pedestal temperature $T_{i,\rm ped}$ (eV). The yellow shade highlights the H-mode phase of #62430 until the loss of confinement due to core radiative collapse.

These findings are illustrated in more detail in figure 14, showing selected time traces of two plasma discharges at 0.87 MA/1.17 T (pulse 62428 in red (dotted in b/w version), and pulse 62430 in blue (full line in b/w version)). After a very similar initial H-mode transition and long ELM-free phase, the NB power was stepped up at about 24 s in #62428 by ∼1 MW, while it was kept constant for 1 s longer in #62430. The power increase in #62428 has two clear effects: $T_{i,\rm ped}$ increases and the pedestal goes into a standard Type I ELM phase; at the same time, the average plasma density and core radiation level off and the plasma reaches stationary conditions. In contrast, the delayed power step up in #62430 corresponds to a short Type III ELM phase followed by an ∼1.5 s (or $\sim 4\tau_E$) period with approximately constant $n_{\rm ped}$ and $T_{i,\rm ped}$ and no Type I ELMs. The continuous rise in the core radiation keeps the power across the separatrix below that of #62428, even after the power is increased to the same level of #62428, and the pedestal temperature remains at ∼250 eV ($T_{i,\rm ped} \sim 320$ eV for #62428). A close examination of the H_α traces both in the divertor and at the plasma outer midplane for #62430 shows that the typical bursts correlated to Type I ELMs are essentially absent, and only small and irregular oscillations are detected, similar to previous observations in Type II ELM phases of JET mixed Type I–II ELMy H-modes. As characteristic of Type II ELMs, an increase of magnetic turbulence (figure 15) is observed during the quiescent phase of #62430, identified as WB modes, given their broadband characteristics, mode number, frequency and the direction of rotation. A detailed comparison of the MHD fluctuations for ASDEX Upgrade and JET Type II ELMs is found in Stober *et al* (2004). The Type II ELM phase is terminated by the collapse of the plasma core.

Is interesting to note that, in the Type II ELM phase of #62430, the pedestal parameters of the JET discharge are very near to those expected from the identity calculations. In particular, a high value of pedestal collisionality of the ASDEX Upgrade model pulse, $\nu^* \sim 2$ is obtained. It appears that, in these identity conditions, the additional loss mechanism correlated to WB modes is sufficient to stabilize the pedestal density rise and both $T_{i,\rm ped}$ and $n_{\rm ped}$ are constant in time. These are, to date, the only conditions in JET where the increase in WB mode intensity (increased continuous power losses) is sufficient to reach steady-state pedestal density. On the other hand, the power flux carried by Type II ELMs in these conditions is limited, as demonstrated by the pedestal behaviour of #62428: a small increase of $P_{\rm sep}$ results in a standard Type I ELMy edge.

Finally, the operational space for achieving a Type II ELMy edge was further explored by increasing I_p and B_T at constant q. At both 1.2 MA/1.6 T and 1.5 MA/2.0 T a fine power scan was carried out to search for a steady Type II ELM edge, and at the same stable core profiles. Although phases of mixed Type I–II ELMs were obtained at 1.2 MA, for the conditions explored the combination of I_p–B_T–$P_{\rm sep}$ resulting in the steady Type II phase of #62430 seems unique: at any power above the L → H power threshold, complete suppression of ELMs was not obtained (see figure 16), indicating that the operational space for Type II ELMs may close down when the minimum power to obtain an H-mode increases because B_T is increased, possibly related to the increase of the minimum $T_{\rm ped}$ ($T_{\rm ped} \propto B_T^{0.8}$, (Andrew *et al* 2004)) required to sustain an H-mode. This last point is illustrated in figure 17, showing the pedestal collisionality as a function of a normalized pedestal ion temperature, $T_{i,\rm ped}/B_T^{0.8}$. The two full squares represent two time slices during the Type II ELM phase of #62430. Although figure 17 shows that the data points from the phase with steady pedestal parameters and Type II ELMs lie in the region of this operational space corresponding to high ν^* and low $T_{\rm ped}$, as expected, it also shows that a clear boundary separating out these points from the others is not identifiable from these data.

3. Small ELM regimes at high β_p

This section describes the behaviour of the pedestal and ELMs in high-β_p H-mode plasmas. As outlined in section 1.1, the possible effect of β_p on ELM behaviour was investigated by carrying out a β_p scan in ELMy H-modes, in a QDN configuration. The experiments were carried out in plasmas with a fully penetrated current profile and no ITB, with $l_i > 1$ for $\beta_p > 1.3$. The plasma shape was QDN, with $\Delta_{\rm sep} \sim 1$ cm (high-l_i/high-β_p configuration, $\delta \sim 0.45$, table 1). In this experiment, β_p was increased in steps from 1.1 to 1.9, by increasing the input power (combined NB and H minority central ICRH) and, at the maximum input power, reducing the plasma current at fixed field. In particular, the toroidal field was fixed at $B_T = 2.7$ T to optimize fast ECE profile measurements, and the plasma current varied from 1.5 to 1.35 and finally down to 1.2 MA. In this scan, q_{95} varied from ∼5 to ∼7, with the highest q_{95} corresponding to the discharges with

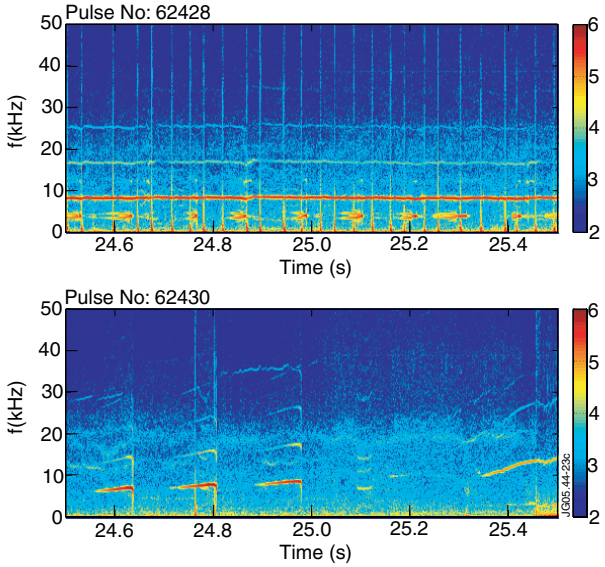

Figure 15. MHD spectrograms for the two plasma discharges #62428 (top) and #62430 (bottom). The spectrogram for #62428 is typical of a Type I ELMy H-mode, while that of #62430, shows WB modes (continuous fluctuations in the 10–25 kHz range) replacing the Type I ELM signature (the short, intense bursts of MHD are due to sawteeth).

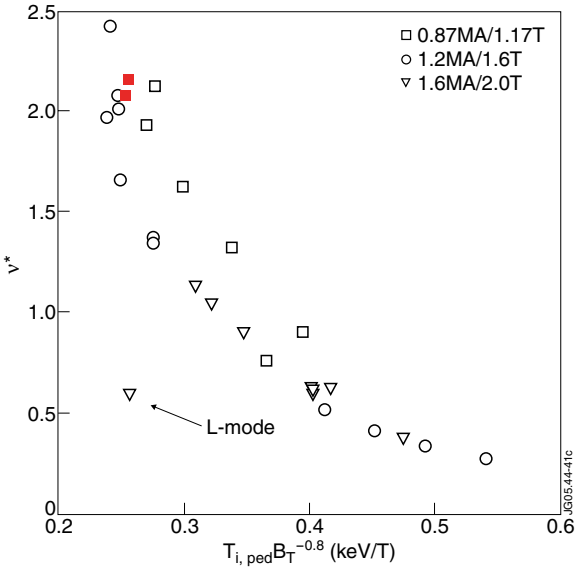

Figure 17. Pedestal collisionality versus pedestal ion temperature normalized to $B_T^{0.8}$, for the ASDEX Upgrade similarity experiments. The full squares represent 2 time slices during the Type II ELM period of #62430.

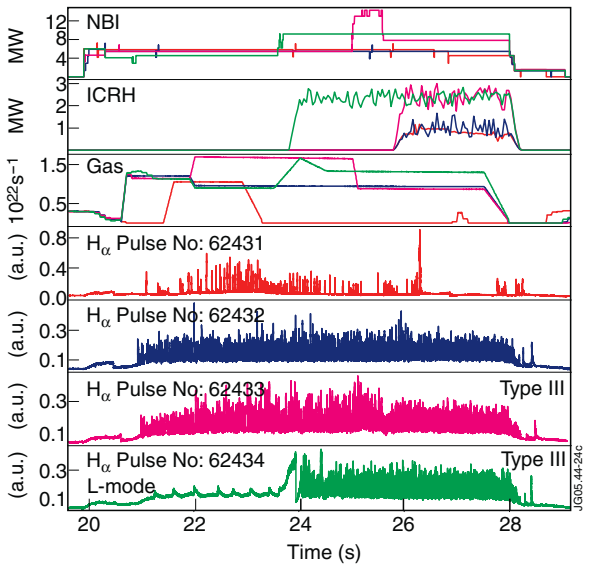

Figure 16. Selected time traces for the power/gas scans carried out in the ASDEX Upgrade similarity experiments, for the 1.5 MA/2 T case, four pulses. Variation of injected power and fuelling were carried out in each pulse to explore the possible access to steady-state Type II ELMy edge, not obtained. From top to bottom: NB injection power (MW), ICRH injected power (MW), gas injection (10^{22} s^{-1}), and divertor H_α traces for each of the four discharges.

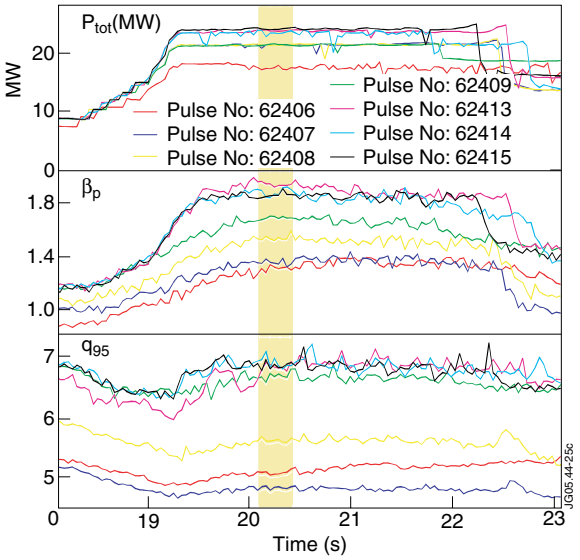

Figure 18. Selected time traces for seven plasma discharges of the high-β_p/high-l_i H-mode scan. From top to bottom: total input power (NBI + ICRH, MW); β_p and q_{95}. The yellow stripe marks the time slice of the zoomed H_α traces in figure 19.

the highest β_p. The total input power, β_p, and edge safety factor q_{95} for seven representative discharges of the series are shown in figure 18, while the corresponding divertor H_α traces (enlarged for clarity) are in figure 19.

At lower input powers, up to $\beta_p \sim 1.5$, the ELM H_α signature is typical of a Type I ELMy H-mode edge: distinct spikes with frequency increasing with input power. At $\beta_p \sim 1.65$ (#62409 at 1.2 MA/2.7 T, $q_{95} \sim 6.5$), a change in the ELM activity is observed, with long phases where the H_α spikes disappear at constant plasma confinement. When β_p is increased further ($\beta_p \sim 1.8$–1.9), regular ELM activity is no longer detectable in the divertor H_α signature: Type I ELM completely disappeared to be replaced by high frequency, very small and irregular oscillations, strongly reminiscent of the grassy ELMs of JT-60U (Kamada *et al* 2002). This change in the ELM behaviour occurs at high confinement ($H_{98} \sim 1.0$–1.2) and high density ($n \sim 85\% n_{GR}$). Both pedestal and core profiles are in steady state, indicating that edge losses associated to these small ELMs are sufficient to

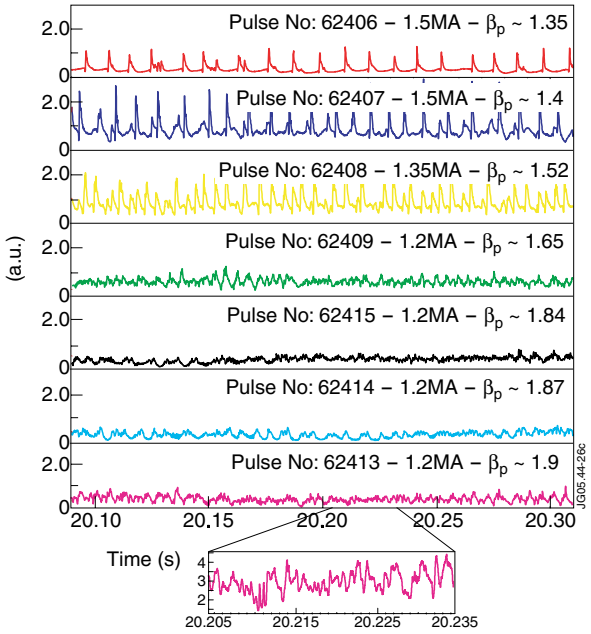

Figure 19. Divertor H_α time traces for the β_p scan in high-l_i H-modes (same plasma discharges and colour code as figure 18). 'Grassy' ELMs are observed for $\beta_p \gtrsim 1.6$–1.7. The 35 ms zoom of the H_α trace of #62413 shows that the regular bursts typical of Type I ELM activity are absent.

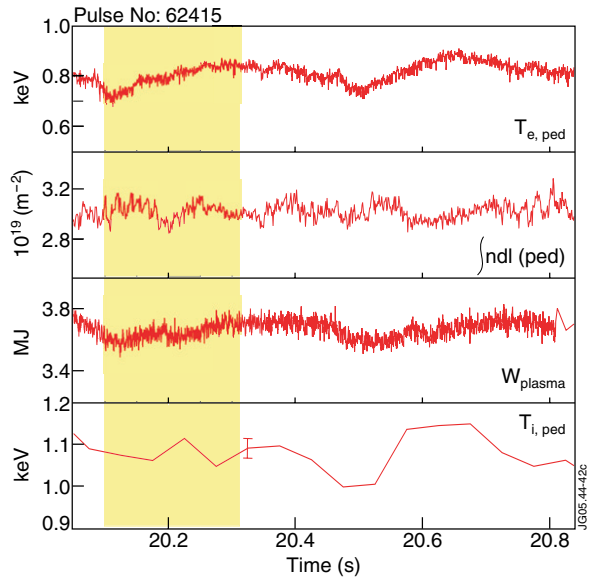

Figure 20. Selected time traces for pulse #62415 ($\beta_p \sim 1.84$) with a grassy ELM edge. From top to bottom: pedestal electron temperature (keV), pedestal n_e (line integrated, 10^{19} m^{-3}), plasma stored energy (MJ) and pedestal ion temperature (keV). The yellow stripe highlights the time interval shown in figure 19.

carry all the power and particles normally lost by Type I ELMs. An example of the time evolution of some pedestal and global plasma parameters is shown in figure 20, for the particular case of the high-β_p pulse #62415. Moreover, grassy ELMs are compatible with high global confinement, with the highest confinement ($H_{98} \sim 1.2$) obtained at the highest β_p. Changes in the MHD fluctuation pattern accompanying the change in the ELM H_α signature, are shown in figure 21, for #62406 (Type I ELMs, $\beta_p \sim 1.35$), and figure 22, for #62413 ('grassy' ELMs, $\beta_p \sim 1.9$). Although fast magnetic measurements are available up to 1 MHz frequency, the figures include only fluctuations in the 0–50 kHz range, to make the features of the grassy ELMs MHD visible. The comparison of the two MHD spectrograms shows that small MHD bursts are still associated with grassy ELM activity, in a way that is reminiscent of the standard MHD signature of Type I ELMs, although the extent in frequency of the MHD perturbation is dramatically reduced compared to Type I ELMs. The time resolution of the available magnetic measurements does not allow us to temporally resolve the small burst observed in the 0–10 kHz range to establish a firm correlation between the irregular H_α spikes of the grassy ELMs and magnetic bursts. Nonetheless, the more important feature of the spectra of grassy ELMy H-modes is the virtual absence of MHD fluctuations above 10 kHz. In particular, in contrast to Type II ELMs, WB modes are not observed in the grassy ELM discharges; this absence of MHD activity with grassy ELMs is also a typical observation in JT-60U (Stober *et al* 2004).

To understand the reasons for the change in ELM behaviour at high β_p observed in the high-l_i H-modes, these discharges are compared to standard ELMy H-modes at low β_p ($\beta_p < 1$) (Loarte *et al* 2004), as well as to a series of discharges carried out at 1.2 MA/2.7 T (like most of the high-l_i H-modes), and where β_p was varied over a similar range, from ~1.1 to ~1.9. In this latter experiment, lower hybrid pre-heating and early main heating were used to control the q profile, and resulted in plasmas with $q_0 > 2$ and a broad current profile ($l_i \sim 0.85$), with some of these discharges having a weak ion ITB. The discharges in this series are identified as 'low-l_i/high-β_p' H-modes (see table 1). These plasmas are standard lower SN ($\Delta_{sep} \gtrsim 4$ cm), with the same δ, κ and similar q_{95} as the QDN used for the high-l_i/high-β_p H-modes. The time traces of total input power (also NB and ICRH combined heating, as for the high-l_i H-modes), β_p and q_{95} are shown in figure 23, while the corresponding divertor H_α traces are shown in figure 24: in contrast to the high-l_i/high-β_p case, increasing β_p does not cause a change in the ELM behaviour, and Type I ELMs are observed up to the highest β_p. Furthermore, MHD spectrograms show the typical Type I ELM signatures, consistent with the H_α traces.

3.1. Confinement and pedestal characteristics of high-β_p H-modes

In this section, the global plasma confinement and pedestal behaviour are analysed, to identify differences and similarities in the high β_p, high- and low-l_i H-modes, which may explain the observed difference in ELM behaviour.

The global plasma confinement of the two series of high β_p is compared in figure 25, showing the confinement enhancement factor H_{98} as a function of the normalized pedestal density n_{ped}/n_{GR}. At low β_p, the low-l_i H-modes have reduced H_{98} compared to both standard Type I ELMy H-modes of that density and high-l_i H-modes ($H_{98} \sim 0.7$–0.9), but for $\beta_p > 1.5$, the global confinement of high- and low-l_i plasmas is very similar, with $H_{98} \sim 1.1$–1.2 in both cases.

The pedestal pressures of the two groups of high-β_p plasmas are compared in figure 26. Since some of the

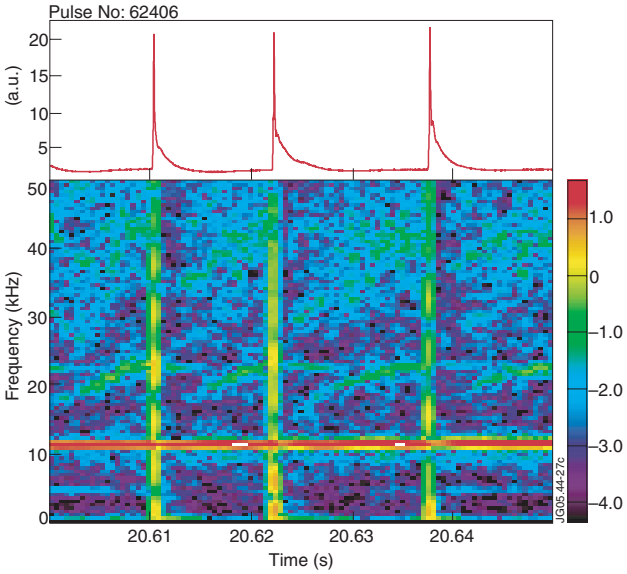

Figure 21. H_α time trace and MHD spectrogram for #62406 (Type I ELMs, $\beta_p \sim 1.35$).

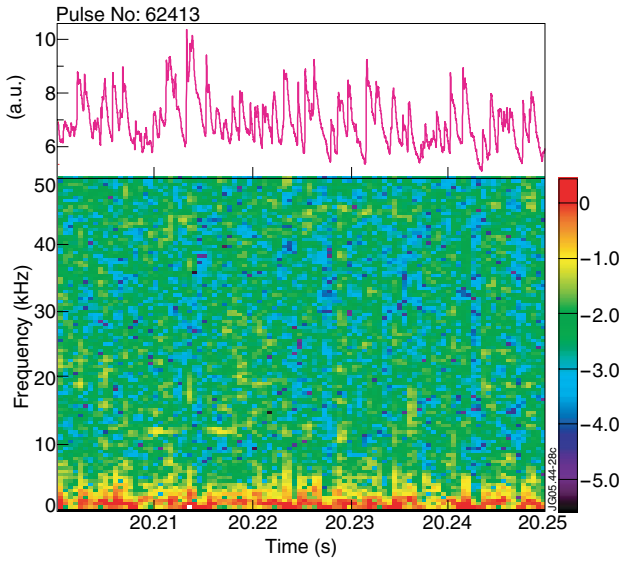

Figure 22. H_α time trace and MHD spectrogram for #62413 (grassy ELMs, $\beta_p \sim 1.9$).

plasmas of the high-l_i series had $I_p \neq 1.2$, $p_{\rm ped}$ in figure 26 is normalized, to allow a direct comparison of all the data (normalization to I_p^2 (Loarte *et al* 2004), to 1.2 MA). In the case of the high-l_i H-modes, $p_{\rm ped}$ is essentially constant with β_p, indicating that the onset of the small and high-frequency grassy ELMs does not reduce the pedestal energy content, in contrast to what is observed at the Type I $\rightarrow$ Type III ELM transition (Sartori *et al* 2004b). For the low-l_i H-modes, $p_{\rm ped}$ increases with β_p, consistently with the global plasma confinement behaviour and, for $\beta_p \sim 1.9$, $p_{\rm ped}$ is very similar to that of the high-β_p high-l_i H-modes. Figure 26 also shows a potentially important difference between the two groups of plasma discharges, namely that the pedestal of the high-l_i H-modes is more collisional than that of the low-l_i H-modes. In particular, this difference is the largest at high β_p: the high-l_i

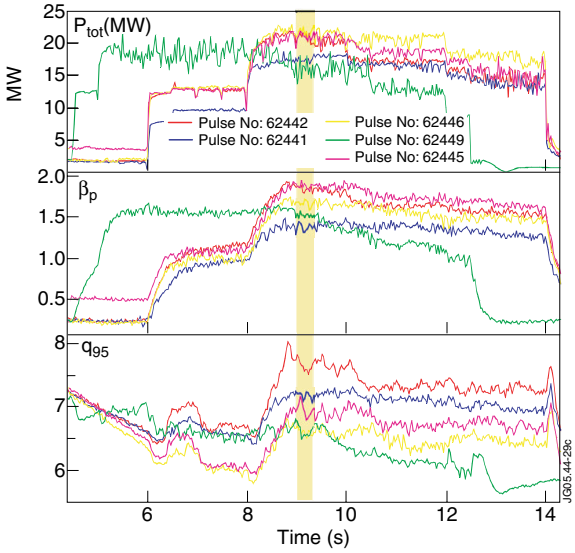

Figure 23. Selected time traces for six plasma discharges of the high-β_p low-l_i H-mode scan. From top to bottom: total input power (NBI + ICRH, MW); β_p and q_{95}. The yellow stripe marks the time slice of the zoomed H_α traces in figure 24.

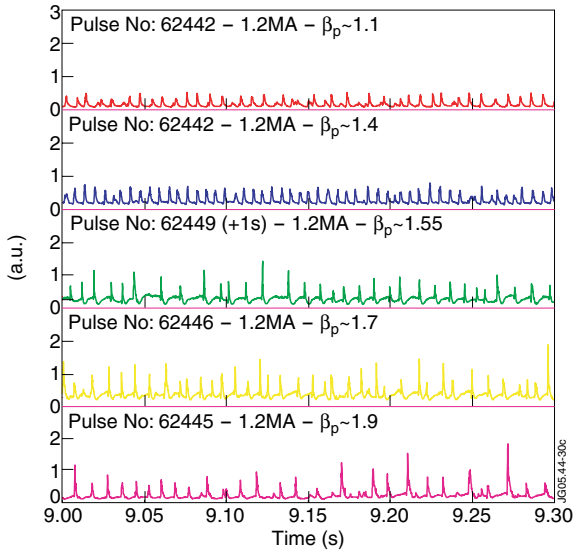

Figure 24. Divertor H_α time traces for the β_p scan in low-l_i H-modes (same plasma discharges and colour code as figure 23). Type I ELMs are observed for all values of β_p.

plasmas with grassy ELMs have pedestal e–e collisionality $0.4 \lesssim \nu^* \lesssim 0.7$ for $1.7 \lesssim \beta_p \lesssim 1.9$, compared to that of the low-l_i plasmas that, in the same range of β_p, have $\nu^* \sim 0.2$. This difference is due to operational reasons: all the high-β_p high-l_i H-modes have strong edge fuelling, to obtain pedestal densities in the range of $\sim 70\% n_{\rm GR}$. The fact that grassy ELMs are only observed above $\nu^* \sim 0.4$, therefore, does not, in principle, represent an 'existence limit' in ν^* for these ELMs, but only reflects the range of pedestal parameters investigated so far.

3.2. Comparison of Type I and 'grassy' ELM losses

The relevance of achieving a 'grassy' ELM edge at high plasma confinement depends on the reduction of bursty ELM losses: in

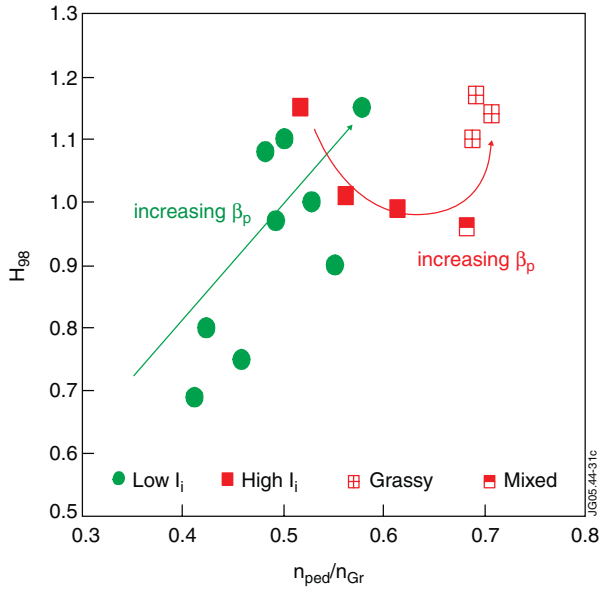

Figure 25. Confinement enhancement factor H_{98} as function of the normalized pedestal density $n_{\rm ped}/n_{\rm GR}$, for both high- and low-l_i H-modes. Full symbols represent data points from H-modes with a Type I edge, half-full symbols are for H-modes with mixed periods of Type I and grassy ELMs, while the squares with crosses represent data points taken with a grassy ELMy edge. This symbol convention is maintained for all subsequent figures.

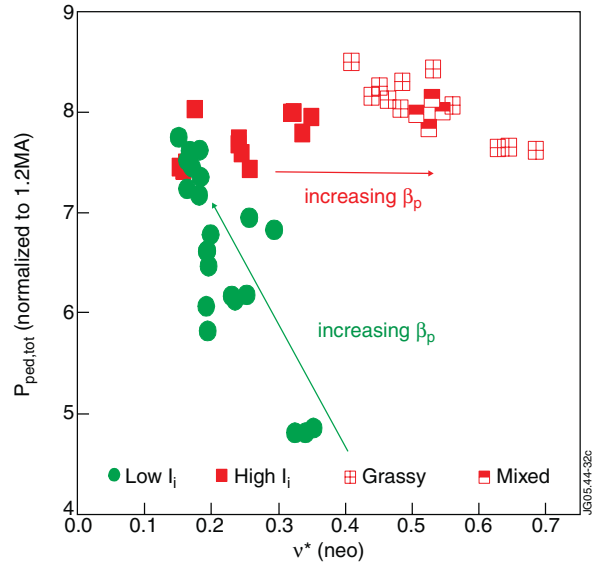

Figure 26. $p_{\rm ped}$ (normalized to I_p^2) for the high-l_i and low-l_i H-modes β_p scans.

fact, although the H_α pattern would indicate that the grassy ELMs are small, a quantitative evaluation of energy losses associated to the small and irregular H_α bursts is required to judge the value of this regime for future development.

Prompt ELM energy losses, temperature and density drop at ELMs were analysed for both high- and low-l_i H-modes and compared to the existing JET database from standard ELMy H-modes (Type I and Type III, $\beta_p \lesssim 1$ (Loarte *et al* 2004)). The results of this analysis are summarized in figures 27(*a*)–(*c*). Figure 27(*a*) shows the ELM energy losses $\Delta W_{\rm ELM}$, normalized to the pedestal energy $W_{\rm ped}$; figure 27(*b*) shows, for the same set of discharges, the pedestal electron temperature drop at the ELM, $\Delta T_{\rm ELM}$, normalized to $T_{e,\rm ped}$ and, finally, figure 27(*c*) shows the pedestal density drop at the ELM, $\Delta n_{e,\rm ELM}$, normalized to the pedestal electron density n_e. Energy losses, temperature and density drop all give the same picture: the high-l_i H-modes ELM losses are comparable to those of standard H-modes up to $\beta_p \sim 1.5$, that is, when they exhibit a Type I ELM edge. At higher β_p, the energy loss associated with 'grassy'; ELMs is very small, below the detection limit (~50 kJ), and corresponds to a maximum of $\Delta W_{\rm ELM}/W_{\rm ped} \sim 4$–5%. These losses below detection limit are represented by the red bars, where the top of the bar represents the maximum estimated loss. The low energy losses with grassy ELMs are confirmed by the analysis of $T_{e,\rm ped}$ and $n_{e,\rm ped}$ drops. Note that the high resolution of the ECE and of the interferometer used for this analysis allow us to resolve ELMs ΔT and Δn that are too small for the fast stored energy loss measurements. Figures 27(*b*) and (*c*) show that both temperature and density drop for grassy ELMs are below those of Type I ELMs with similar ν^*, and even lower than those measured for Type III ELMs, in spite of the global confinement and pedestal pressures with grassy ELMs being similar or higher than expected for a Type I ELMy H-mode. In contrast, ELM losses of the low-l_i H-modes are similar to those of standard Type I ELMs, although the lack of data on the ELM density losses does not allow a more detailed comparison.

The reduction of the size of grassy ELMs compared to Type I ELMs may be explained by comparing the ELM affected depth, $L_{\rm ELM}$. $L_{\rm ELM}$ is estimated from the radial extent of the prompt perturbation of the radial T_e profile caused by an ELM. The perturbed T_e profile is obtained by subtracting the post-ELM T_e profile from the pre-ELM T_e profile, dividing the difference profile by the initial $T_e(r)$ and then normalizing this profile to its maximum.

Figures 28(*a*) and (*b*) compare $L_{\rm ELM}$ for two groups of data: figure 28(*a*) shows the perturbed T_e profiles for a density scan in standard H-modes (at fixed I_p, B_T, shape and $P_{\rm in}$), including both Type I and Type III ELMs; although increasing the density (ν^*) reduces ELM energy losses by a factor ~3 (or ~2 when normalized to $W_{\rm ped}$), the ELM affected depth does not change significantly as long as the pedestal maintains Type I ELMs. Figure 28(*b*) compares $L_{\rm ELM}$ for ELMs from two plasmas in the HT3 configuration at low and medium q_{95} (~3.6 and ~4.5, from the same series of discharges described in section 2.1) and shows that, although increasing q_{95} from ~3.6 to ~4.5 reduces Type I ELM losses very significantly (by a factor of 3–4), $L_{\rm ELM}$ again remains the same. A reduction of ELM size accompanied by a reduction of the ELM affected depth is observed only in the case of Type III ELMs (figure 28(*a*), open symbols), that is for ELMs that are probably caused by a different MHD instability than Type I ELMs, (Loarte *et al* 2004). These observations can be contrasted with the behaviour of $L_{\rm ELM}$ in the high-l_i H-mode β_p scan, shown in figure 29(*a*). In this case, one sees that the reduction of the ELM losses observed with grassy ELMs at high-β_p corresponds to a shrinking of the ELM affected depth, strongly suggesting that a change in the MHD instability or consequent relaxation in the pedestal may be at the root of the reduction in the ELM size. Such a reduction of $L_{\rm ELM}$ with β_p is

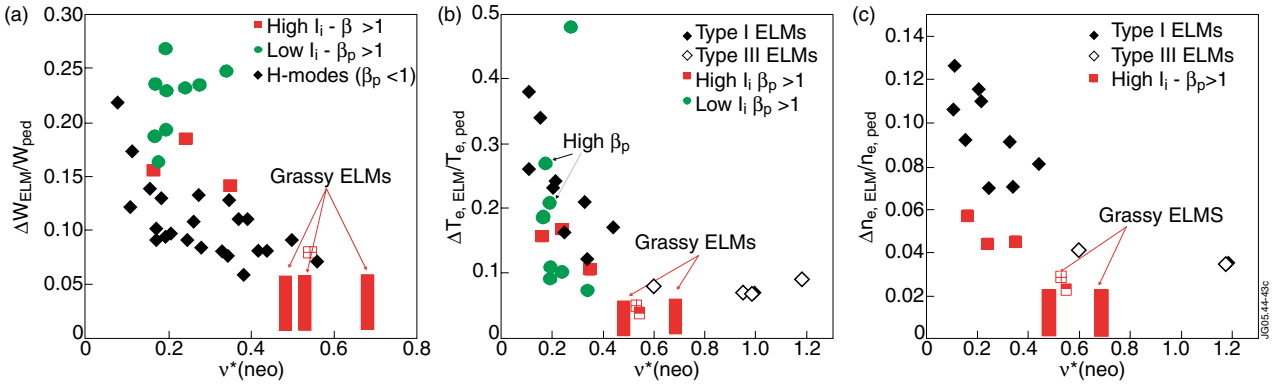

Figure 27. Summary of ELM losses for high-β_p/high-l_i, high-β_p/low-l_i and standard ($\beta_p < 1$) H-modes. (*a*) ELM energy losses $\Delta W_{\rm ELM}$, normalized to the pedestal energy $W_{\rm ped}$; (*b*) pedestal electron temperature drop at the ELM, $\Delta T_{\rm ELM}$, normalized to $T_{e,\rm ped}$; (*c*) pedestal density drop at the ELM, $\Delta n_{e,\rm ELM}$, normalized to the pedestal electron density n_e. Fast density measurements were not available for the low-l_i H-modes. In all figures, standard H-modes are in black diamonds (from Loarte *et al* (2004)), low-l_i H-modes are in green dots, and high-l_i H-modes are in red squares. The red bars are calculated from estimated $\Delta W_{\rm ELM}$, $\Delta T_{\rm ELM}$ and $\Delta n_{\rm ELM}$, with the top of the bar being the upper value for those quantities.

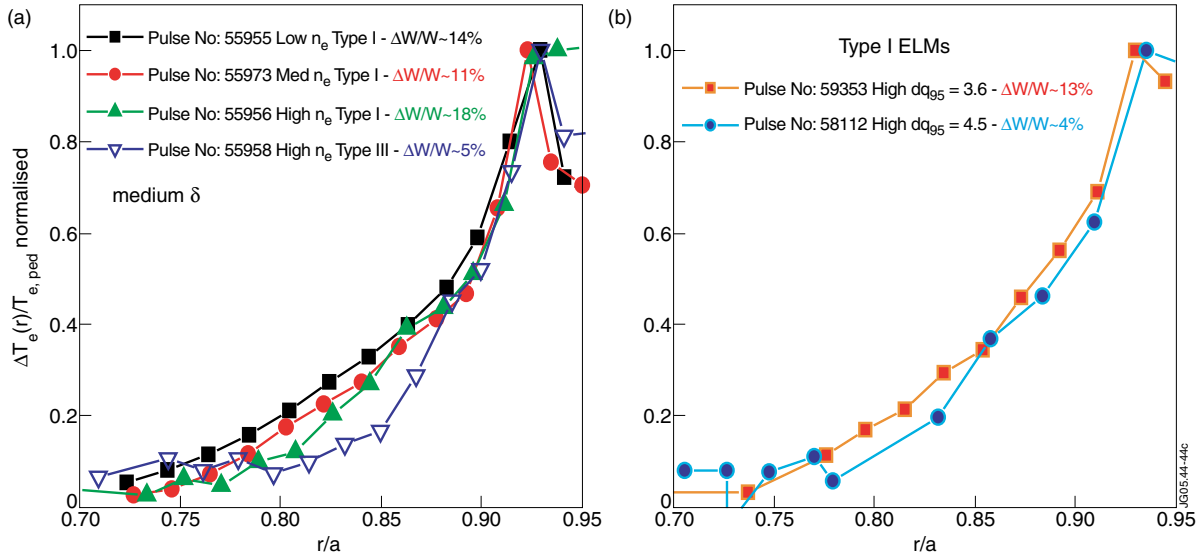

Figure 28. Perturbed T_e profiles for several H-mode discharges. (*a*) Density/gas scan in a medium δ ELMy H-mode at 2.5 MA/2.4 T, at constant $P_{\rm in}$; full symbols Type I ELMs, open symbols, Type III ELMs. (*b*) Comparison between the temperature profile perturbation of 2 HT3 discharges at $q_{95} = 3.6$ and $q_{95} = 4.5$, both with Type I ELMs.

not observed for the low-l_i H-modes (figure 29(*b*)), which are similar in this regard to standard H-modes, as may be expected, since they maintain a Type I ELMy pedestal. Finally, figures 28 and 29 also show that $L_{\rm ELM}$ of the high-l_i H-modes is smaller than both standard H-modes and low-l_i H-modes. This would indicate that the shrinking of the ELM affected area is not a pure high-β_p effect, and further supports the idea of a change in the pedestal MHD stability.

4. Discussion

As shown in section 2, a steady-state H-mode with Type II ELMs and complete Type I ELM suppression has not been achieved in JET for the normal JET plasma operating conditions (medium current $I_P \sim$ 2–3 MA, $q_{95} \sim$ 3–3.6). However, at high shaping and density, mixed phases of Type I–II ELMs are observed regularly and reproducibly, both in SN and QDN plasmas. It has been shown that, in contrast to indications from other experiments, increasing q_{95} both in SN and QDN, from ~3 to ~4.5 (by varying either I_p or B_T), does not facilitate the access to the Type II ELM regime (section 2.1). Moreover, increasing q_{95} affects the pedestal behaviour in the Type I ELM regime: the Type I ELMs frequency is much higher than at $q_{95} \sim 3$, no clear Type II ELM phases are detected, and Type I–III ELM transitions occur at lower pedestal density than at lower q_{95}.

The interpretation of these results in terms of changes of the ideal MHD stability of the pedestal is not straightforward and unequivocal. In Lonnroth *et al* (2004) an MHD ELM model is put forward to interpret the changes in ELM type observed in experiments for increasing density, variation of the edge safety factor, β_p and shape. In this model, Type I ELMs occur when the pedestal is in the second stability region (to $n = \infty$ ballooning modes), and are caused by the

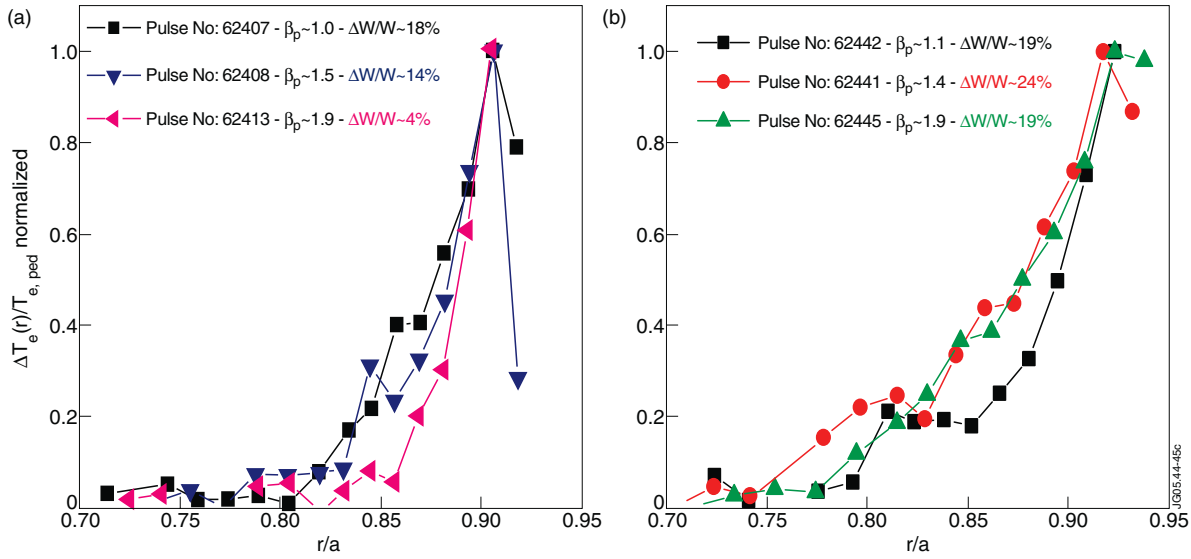

Figure 29. Perturbed T_e profiles for several H-mode discharges at high β_p. (*a*) Three pulses of the β_p scan, high l_i and (*b*) three pulses of the β_p scan, low l_i.

pedestal gradients reaching a finite-n ballooning stability limit. In contrast, Type II ELMs are assumed to originate from a different MHD instability, namely ideal $n = \infty$ ballooning modes. Mixed Type I–II regimes are interpreted as being the result of different zones of the pedestal being dominated by a different instability: the inner part of the pedestal region is in the second stability regime, and large perturbations (Type I ELMs) occur when the finite-n ballooning limit is reached, while the outer part of the pedestal is instead $n = \infty$ ballooning unstable (and limited to a lower critical pressure gradient), and smaller and more frequent ELMs (Type II) are, therefore, generated when this limit is reached. This model has been applied to the comparison of MHD stability of high-δ, high-κ SN and QDN plasmas both in predictive and interpretative simulations (using experimental profiles from discharges with the same I_p, B_T and input power) with the JETTO–MISHKA suite of codes. It is found that the variation of the magnetic geometry from SN to QDN does not change the MHD stability of the pedestal in a qualitative way, and the access to the mixed Type I–II regime is similar in both cases. In the simulations, the experimental fact that plasmas with QDN magnetic geometry tend to reach higher n_{ped} than similar SN plasmas has a stronger effect on the access to the Type I–II regime than magnetic geometry alone. These results are in qualitative agreement with the experimental findings reported in this paper, in particular with the observations that the longest Type II ELM periods are observed in QDN plasmas, as well as the fact that the largest increase in inter-ELM losses is the mixed Type I–II regime (see figure 12(*b*)). In contrast, MHD stability analysis of the ASDEX Upgrade Type II ELMy H-modes, carried out with the IDBALL and GATO codes (Saarelma *et al* 2003), showed that the combination of proximity to double null and high q_{95} has a clear effect on the pedestal stability. In particular, approaching double null configuration, at high density and q_{95}, has the effect of stabilizing low-n peeling/ballooning modes and increasing the localization of the modes in the edge region. This is found to be in qualitative agreement with the change from Type I to Type II ELMs observed in ASDEX Upgrade under those experimental conditions. These two (apparently) contradicting results (QDN does not facilitate access to Type II ELMs in Lonnroth *et al* (2004), while it does in Saarelma *et al* (2003)) may be partially understood by noting that the two authors attribute different MHD modes to Type II ELMs: for Lonnroth *et al* (2004), Type II are ideal ballooning modes, while for Saarelma *et al* (2003), the signature of Type II ELMs is that the most unstable modes are high-n peeling–ballooning (P–B) with shrinking eigenmode widths (compared to a reference Type I ELMy H-mode case). Detailed inter-machine comparison is probably needed to clarify this issue, as well as to identify any artefacts in the results that may be due to the different spectral resolution of the codes used in the analysis.

The ELM model in Lonnroth *et al* (2004) was also applied to the study of the effects of q_{95} on pedestal and ELM stability. The simulations find that increasing q_{95} increases the magnetic shear in the edge, and also changes the $n = \infty$ ballooning stability limits in the edge region, and the combination of these two effects is indeed favourable to the onset of Type II ELMs. Although this modelling result is consistent with findings from other devices, it does not reflect the experimental observations for JET plasmas. The observed variation of Type I ELM size and frequency with q_{95} is analysed by Saarelma *et al* (2004), for the case of JET pulses of fixed shape (medium δ) and varying q_{95}: in this case, it is found that the dominant instabilities are low to intermediate-n P–B modes, and that increasing q_{95} 'moves' this limit to higher values of the normalized pressure gradient (and to higher values of the pressure gradient itself). Interestingly, increasing q_{95} has very little effect on the radial extent of the most unstable modes, indicating that the change in ELM frequency and size is not due to a change in the structure of the triggering instability, in agreement with experimental observations.

H-modes with pure Type II ELM edge and constant n_{ped} and T_{ped} were indeed obtained in JET/ASDEX Upgrade Type II ELM identity conditions. Unfortunately, since these experiments were carried out at a low I_p, the quality of the edge

profile measurement is not sufficient for a meaningful MHD stability analysis; nonetheless, these experiments may give some indications on possible physics mechanisms of Type II ELMs. In particular, the observation that any increase in input power and/or current and field results in Type I and Type III ELMy H-mode edge suggests that the amount of power and particle exhaust carried by 'continuous' transport due to the Type II ELMs is limited, with this loss mechanism possibly being associated to low pedestal temperature or high collisionality regimes (see Perez *et al* (2004), Stober *et al* 2004). The association between increased edge losses, pedestal dynamics, and WB modes also suggests the idea of including WB modes in the standard P–B model for the pedestal MHD stability (Connor *et al* 1998, Snyder *et al* 2002), at this stage, conceptually. This idea is developed in detail in Perez *et al* (2004): while an ELM is triggered, in the P–B model, only when the pedestal becomes peeling unstable, in the ELM cycle model including WB modes assumes that the ELM instability is pressure driven. Since WB modes are unstable at low pressure (well below the ballooning limit), and lead to increased inter-ELM transport, they may increase the time required to reach the critical pressure gradient triggering the ELM and, in particular cases (high ν^* or low $T_{\rm ped}$), avoid it entirely. This picture is qualitatively consistent with experimental observation in JET. A substantiation of this argument certainly requires the identification of the nature of WB modes, which is still an open issue at the moment. Finally, transport simulations were carried out of the JET/ASDEX Upgrade identity discharge #52430, where long Type II ELM phases were found, and compared to simulations of other discharges in the same series, where Type I ELMs were still observed. For these particular conditions, transport analysis indicates that the high pedestal collisionality drives very high neoclassical losses, which in the simulations allow the pedestal to reach steady state before reaching the Type I ELM MHD limit. Although these simulations reproduce the experimental data only in a qualitative way, they again point towards a link between high collisionality and Type II ELMs.

The most successful scenario to date for obtaining small ELMs and simultaneous high pedestal pressure and confinement in steady state in JET is the combination of high shaping (in this case QDN), high β_p ($\beta_p \gtrsim 1.65$) and high q_{95}. There are several similarities in the phenomenology of the grassy ELMy H-modes in JET and in JT-60U, in particular the existence of a threshold value for the global β_p for the onset of these ELMs. On the other hand, the comparison of the ELM behaviour of high-l_i and low-l_i H-modes at high β_p (section 3) would indicate that, for the case of JET, high β_p is possibly a necessary but not sufficient condition for obtaining a grassy ELMy H-mode edge. One possible explanation for the change in ELM character at high β_p, put forward for the JT-60U grassy ELM plasmas (Kamada *et al* 2002, Kamada and the JT-60U Team 2001), is that grassy ELMs are the result of a change in the ideal MHD stability of the pedestal, caused by the compression of the magnetic surfaces in the edge due to a strong Shafranov shift (Δ_S). This mechanism for the change in the P–B stability of the pedestal is also put forward by Saarelma and Guenter (2004), in combination with high-δ effects, for the interpretation of the effect of high β_p on pedestal and ELMs in ASDEX Upgrade discharges.

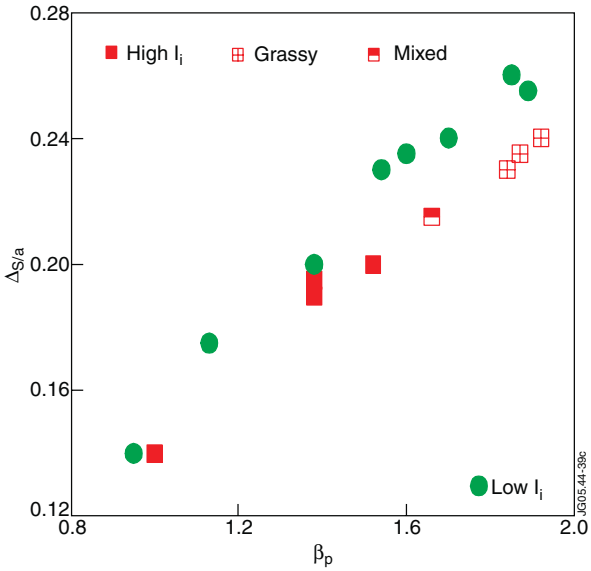

Figure 30. Shafranov shift (normalized to the plasma minor radius) Δ_S/a as a function of β_p, for the β_p scan in the high-l_i (squares) and low-l_i H-modes (circles).

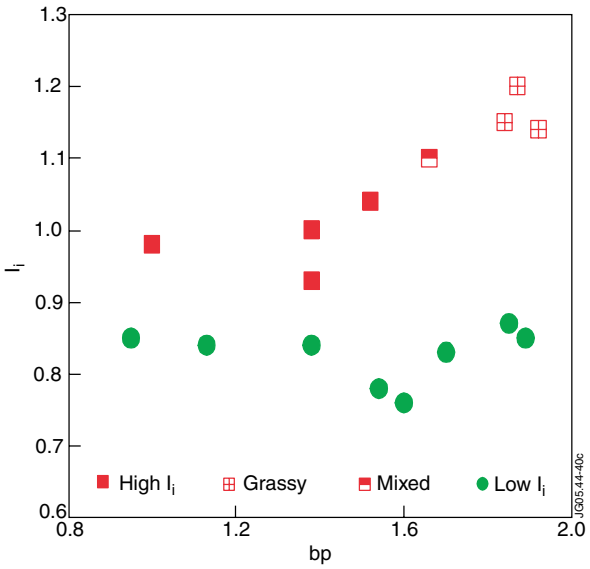

Figure 31. Internal inductance l_i as a function of β_p, for the same set of discharges in figure 30.

In the case of the high-β_p experiments in JET, Δ_S for both high- and low-l_i H-modes is shown in figure 30, as a function of β_p. Δ_S is quite high in both cases, reaching values ~22–26% of the minor radius for $\beta_p \gtrsim 1.7$. Nonetheless, grassy ELMs are observed only for the high-l_i H-modes. This observation suggests that other factors contribute to the change in stability of the pedestal at high β_p: one possible contribution may come from the differences in the current profiles of the two groups of high-β_p discharges, as illustrated in figure 31. Grassy ELMs are observed at high β_p in discharges with a rather peaked current profile ($l_i \gtrsim 1.1$), compared to the companion plasmas at the same β_p but with a broader current profile ($l_i \lesssim 0.85$), at the same total plasma current. One may speculate that the contribution of the inductive current to

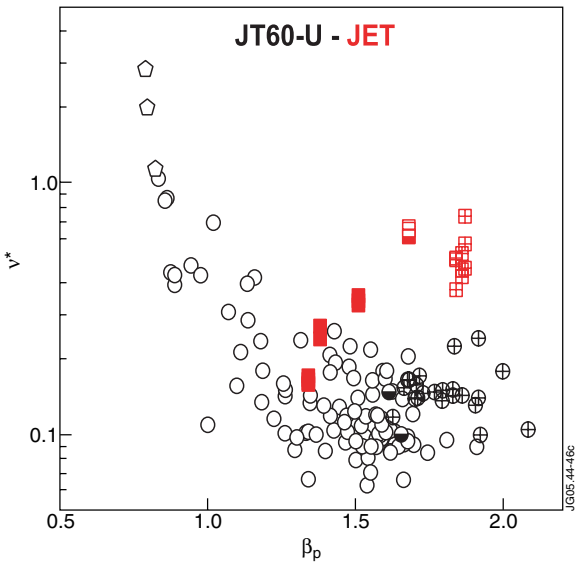

Figure 32. Pedestal collisionality versus β_p, for H-modes in JET (red squares) and JT-60U (black dots). JT-60U: open dots: Type I ELMs; half-full dots: mixed Type I/grassy; dots + crosses: grassy ELMs. JET: full squares: Type I ELMs; half-full squares: mixed Type I/grassy; squares + crosses: grassy ELMs. Note that the increase of ν^* with β_p for the JET data is due to increasing q_{95}.

the edge current will be smaller in case of high l_i, reducing the total amount of toroidal current in the edge and, therefore, improving the pedestal stability against low- medium-n P–B modes (this mechanism is invoked by Saarelma and Guenter (2004) in the case of high-β_p H-modes in ASDEX Upgrade). It is interesting to note that both Saarelma and Guenter (2004) and Lonnroth *et al* (2004) find that increasing β_p changes the stability of the pedestal towards a more ballooning type of instability. Of course, ν^* is another important factor that can affect the current density in the pedestal region and, as shown in figure 26, at high β_p the high-l_i H-modes have higher pedestal collisionality than the low-l_i H-modes. Nonetheless, the minimum ν^* for which steady-state grassy ELMs have been obtained is relatively low, $\nu^* \sim 0.4$, compared to $\nu^* \sim 2$ of the Type II ASDEX similarity pulse #62430 (section 2.4). To investigate further the role of collisionality in obtaining grassy ELMs, we compare the high-l_i H-modes to low-l_i H-modes at the same β_p ($\nu^* \sim 0.2$) and to typical JT-60U grassy ELM H-modes ($\nu^* \sim 0.1$, figure 32). Using as a crude estimate of the bootstrap current $j_{\rm boot} \propto 1/(1+\nu^*)$, we find that decreasing ν^* from 0.4 to 0.2 (0.1) would increase $j_{\rm boot}$ by only ∼15% (∼20%). This observation indicates that the difference in collisionality between high- and low-l_i H-modes is not likely to be the major factor determining the total edge current, and therefore ν^* is not the prime candidate at this stage to explain the difference in ELM behaviour for high- and low-l_i H-modes. Likewise, the difference in collisionality between JET and JT-60U is probably not sufficient to rule out a common nature of these ELMs in the two devices.

Are Type II and grassy ELMs the same phenomenon? The JET experiments presented in this paper highlight similarities between the two regimes; in particular, both are obtained in JET at high plasma shaping and in a QDN configuration. The same experiments reveal important differences between the two regimes in JET, especially when pure Type II are compared to grassy ELMy H-modes: pedestal collisionality ($\nu^* \sim 2$ compared to $\nu^* \sim 0.4$), and MHD spectra (Type II are associated with strong WB modes increasing transport, while grassy ELMs are characterized by very low MHD fluctuations). Moreover, grassy ELMs have been obtained so far only at very high q_{95}, while increasing q seem to close off access to Type II ELMs in JET. At this stage, the data seem to indicate that Type II and grassy ELMs in JET are probably distinct phenomena.

5. Conclusions and outlook

The access to ELMy H-modes with high confinement and small ELMs has been investigated in detail in JET. It is found that, under standard plasma conditions ($I_P \sim$ 2–3 MA, $q_{95} \sim$ 3–3.6), high shaping ($\delta \gtrapprox 0.4$) and high pedestal density ($n_{\rm ped} \gtrsim 70\% n_{\rm GR}$), the pedestal accesses a mixed Type I–II ELM regime. This regime is observed for both SN and QDN magnetic configurations. Long periods of Type II ELMs (up to 150 ms in QDN) are obtained at high $n_{\rm ped}$, associated with an increase of both magnetic and density fluctuations, compared to levels in Type I ELMy H-modes. Measurements of density fluctuations by interferometry and reflectometry indicate that the location of these enhanced fluctuation regions is likely to be near the pedestal top. Increasing q_{95} from ∼3 to ∼4.5 (by varying either I_p or B_T at constant plasma shape), does not facilitate the access to the Type II ELM regime, in contrast to indications from other experiments. The enhanced ∼20 kHz magnetic fluctuations observed in the Type II ELM periods are identified as strong WB modes, possibly responsible for the increased inter-ELM transport. Power balance calculations do indeed show that the power carried by Type I ELMs is reduced by a factor of 2–3 in the presence of enhanced MHD between ELMs, with $P_{\rm ELM}/P_{\rm sep}$ going from a maximum of 50–60% in Type I ELM discharges, down to 27% in SN plasmas and to 21% in QDN. Evaluation of the inter-ELM refuelling rate shows that enhanced particle losses associated with Type II ELMs are nonetheless insufficient to drive the pedestal to steady state. This would indicate that control of the density rise rate at the plasma edge may be crucial for achieving steady-state Type II ELMs at high confinement, in particular for plasmas near double null ($T_{\rm ped}$ saturates between ELMs). In JET (and ITER), the long absolute particle confinement time may necessitate active control of recycling in the upper x-point region as well as of fluxes from the main chamber/limiters.

The role of QDN magnetic geometry, in achieving Type II ELMs in steady state, was further investigated in JET/ASDEX Upgrade identity experiments (0.87 MA/1.17 T, $q_{95} \sim 4.1$ and $P_{\rm in} \sim 4$ MW). For the first time, long Type II ELM phases, with constant $n_{\rm ped}$ and $T_{\rm ped}$, were obtained with the pedestal parameters matching the identity conditions (in particular, $\nu^* \sim 2$), with the Type II ELM periods being terminated only by core radiative collapse. Strong WB mode activity is observed during the Type II ELM periods, similar to that of the higher current mixed Type I–II plasmas described above. Increasing $P_{\rm in}$ at fixed plasma parameters results in the reappearance of Type I ELMs, indicating that the amount of power/particles that can be exhausted across the separatrix by Type II ELMs under these conditions is rather small. Similar results are found by increasing I_p and B_T at constant q: as soon

as enough power was applied to obtain a H-mode, standard Type III or Type I ELMs reappear. Even with QDN, high ν^* and/or low $T_{\rm ped}$ (resistive MHD) may be required to obtain Type II ELMs and sufficient losses to maintain the pedestal in steady state, casting doubts on the potential for extrapolation of this ELM regime to hot plasmas.

The investigation of the effect of high β_p on the pedestal and ELMs in H-mode plasmas has shown that small and irregular ELMs (grassy ELMs) appear above $\beta_p \sim 1.6$–1.7, in high-l_i H-modes. Grassy ELMs cause very low bursty energy and particle losses, smaller than those measured for Type I ELMs at the same collisionality, pedestal pressure and global confinement, but sufficient to obtain steady state in the plasma pedestal and core. Analysis of the fast perturbation of the temperature profile at the ELM shows that the reduction of ELM losses with grassy ELMs may be attributed to the shrinking of the ELM affected depth. This finding (in contrast to the case of Type I ELMs, where changes in ELM amplitude occur at constant $L_{\rm ELM}$) suggests that the onset of grassy ELMs may be due to a change in the mode(s) making the pedestal MHD unstable. Comparison between low- and high-l_i H-modes indicates that high β_p is a necessary but not sufficient condition for obtaining grassy ELMs.

The operational space for grassy ELMs in JET needs to be explored further and extended, to establish the relevance of this small ELM regime as an ELM mitigation scenario. The conditions of the experiments described in this paper are such that all the high-β_p discharges with grassy ELMs were obtained in plasmas with extremely high safety factor ($q_{95} \sim 6.5$–7) and relatively high pedestal collisionality compared to JT-60U (minimum $\nu^* \sim 0.4$), although these values of q_{95} and ν^* were dictated by experimental constraints (available input power, range of density explored) and do not represent, in principle, an existence boundary for grassy ELM onset. Moreover, a QDN configuration was used for the high-l_i experiments, as opposed to the SN used for the low-l_i H-modes, leaving open the question of the role of magnetic geometry in obtaining this small ELM regime. Future experiments should focus on obtaining high-β_p plasmas at lower ν^* and q_{95}. Under those conditions, the systematic investigation of the role of edge currents and plasma shape in determining the operational space of grassy ELMs would also be required, to clarify the extrapolation potential of this regime.

Acknowledgments

The authors thank all the JET-EFDA collaborators for help in the execution of the experimental programme and in the data analysis. The experiments described in this paper were carried out in the JET-EFDA Task Force S1 and S2 in 2002–2003. The efforts of all members of the Task Force, and of the Task Force Leaders in the organization of the experiments, data analysis and publication of results are gratefully acknowledged. We also thank Dr Y. Kamada (JAERI, Japan) for providing the data used in the calculations of the JT-60U data points in figure 32.

References

Andrew Y. *et al* 2004 *Plasma Phys. Control. Fusion* **46** 337
Chankin A.V. and Saibene G. 1999 *Plasma Phys. Control. Fusion* **41** 913
Connor J.W. *et al* 1998 *Phys. Plasmas* **5** 2687
Cordey J.G. *et al* 1996 *Plasma Phys. Control. Fusion* **38** A67
Evans T.E. *et al* 2004 *Phys. Rev. Lett.* **92** 235003
Federici G. *et al* 2003 *J. Nucl. Mater* **313–316** 11
Greenwald M. *et al* 1988 *Nucl. Fusion* **28** 2199
Kamada Y. *et al* 2002 *Plasma Phys. Control. Fusion* **44** A279
Kamada Y. and the JT-60U Team 2001 *Nucl. Fusion* **41** 1311
Koslowski H.R. *et al* 2003 Relation between Type-II ELMs, edge localized turbulence, washboard modes and energy losses between ELMs in high density ELMy H-modes on JET *30th EPS Conf. on Controlled Fusion and Plasma Physics (St Petersburg, 7–11 July 2003)* vol 27A (ECA) P-1.102
Lang P.T. *et al* 2003 *Nucl. Fusion* **43** 1110
Loarte A. *et al* 2004 *Phys. Plasmas* **11** 2668
Lonnroth J.-S. *et al* 2004 *Plasma Phys. Control. Fusion* **46** 767
Perez C.P. *et al* 2004 *Plasma Phys. Control. Fusion* **46** 61
Ryter F. *et al* 2001 *Nucl. Fusion* **41** 537
Saarelma S. and Guenter S. 2004 *Plasma Phys. Control. Fusion* **46** 1259
Saarelma S. *et al* 2003 *Nucl. Fusion* **43** 262
Saarelma S. *et al* 2005 MHD stability analysis of diagnostic optimized configuration (DOC) shots in JET *Plasma Phys. Control. Fusion* **47** 713
Saibene G. *et al* 2001 The effect of plasma shape on density and confinement of ELMy H-modes in JET *Proc. 28th Conf. on Controlled Fusion and Plasma Physics (Madeira)* vol 25A (ECA) P3.002/Or.28
Saibene G. *et al* 2004 Small ELM experiments in H-mode plasmas in JET *Proc. 31st Conf. on Controlled Fusion and Plasma Physics (London)* vol 28G (ECA) paper O-4.02.
Saibene G. *et al* 2002 *Plasma Phys. Control. Fusion* **44** 1769
Sartori F. *et al* 2005 Magnetic control in a large tokamak: JET *IEEE Control Syst. Mag.* submitted
Sartori R. *et al* 2004a Scaling study of ELMy H-mode global and pedestal confinement at high triangularity in JET *Proc. 20th Fusion Energy Conf. 2004 (November 2004)* (Vienna: IAEA) paper IAEA-CN-116/EX/6-3 and http://www-naweb.iaea.org/napc/physics/fec/fec2004/datasets/index.html.
Sartori R. *et al* 2002 *Plasma Phys. Control. Fusion* **44** 1801
Sartori R. *et al* 2004b *Plasma Phys. Control. Fusion* **46** 723
Sips A.C.C. *et al* 2002 *Plasma Phys. Control. Fusion* **44** A151
Smeulders P. *et al* 1999 *Plasma Phys. Control. Fusion* **41** 1303
Snyder P.B. *et al* 2002 *Phys. Plasmas* **9** 2037
Stober J. *et al* 2004 Small ELM regimes with good confinement on JET and comparison to those on ASDEX-Upgrade, Alcator C-mod, and JT-60U *Proc. 20th Fusion Energy Conf. 2004 (November 2004)* (Vienna: IAEA) paper IAEA-CN-116/EX/P1-4 and http://www-naweb.iaea.org/napc/physics/fec/fec2004/datasets/index.html.
Stober J. *et al* 2001 *Nucl. Fusion* **41** 1123